Supernova progenitors and iron density evolution from SN rate evolution measurements

G. Blanc [a,*], L. Greggio [b]

[a] *Laboratoire APC, 10, rue Alice Domon et Léonie Duquet, 75205 Paris Cedex 13, France.*
[b] *INAF Osservatorio Astronomico di Padova, Vicolo dell'Osservatorio 5, 35122 Padova, Italy.*

Abstract

Using an extensive compilation of literature supernova rate data we study to which extent its evolution constrains the star formation history, the distribution of the type Ia supernova (SNIa) progenitor's lifetime, the mass range of core-collapse supernova (CCSN) progenitors, and the evolution of the iron density in the field.

We find that the diagnostic power of the cosmic SNIa rate on their progenitor model is relatively weak. More promising is the use of the evolution of the SNIa rate in galaxy clusters. We find that the CCSN rate is compatible with a Salpeter IMF, with a minimum mass for their progenitors $\gtrsim 10$ M$_\odot$. We estimate the evolution in the field of the iron density released by SNe and find that in the local universe the iron abundance should be ~ 0.1 solar. We discuss the difference between this value and the iron abundance in clusters.

Key words: supernova: rate, galaxies: chemical evolution, galaxy clusters
PACS: 97.60.Bw, 98.65.Cw, 98.62.Bj

1. Introduction

As the last stage of the evolution of stars in a wide range of masses, supernovae play a unique role in the cycling of matter in galaxy evolution. They release in the interstellar medium all of the iron available in the Universe, which is produced (mainly as radioactive Nickel 56) in the explosion itself (Woosley et al. 2002). The supernova rate (SNR) is then closely related to the rate of Fe enrichment of galaxies and of the universe in general.

There are two main families of supernovae, the "Core-Collapse Supernovae" (CCSN) which regroup into the observational types II, Ib and Ic, and the type Ia SNe (SNIa), which are the product of the thermonuclear explosion of a white dwarf (WD), accreting matter from a companion.

CCSN are the result of the death of massive stars. Modeling the explosion is rather difficult due to the complicated physical processes taking place in the extreme conditions of the collapsing Fe core (see e.g. Woosley & Weaver 1986; Janka et al. 2007). This reflects into an intrinsic difficulty to predict the exact mass range of the progenitors of the different CCSN kinds, as well as of the amount of radioactive nickel released to the interstellar medium by each event. However, there is no doubt that the lifetimes of CCSN progenitors are short, less then a few 10 Myr, which implies that the CCSN rate closely follows the star formation rate.

The main frame of the SNIa theoretical paradigm needs a CO white dwarf in a close binary system. The primary star results from the evolution of an intermediate mass star ($M \lesssim 8$ M$_\odot$) which develops a degenerate CO core. When, due to evolution, the secondary expands and fills its Roche Lobe, the CO WD may accrete and grow in mass, and, if the Chandrasekhar limit is reached, C is ignited under degenerate conditions, initiating a thermonuclear explosion. This is the Single Degenerate (SD) channel for SNIa's production (see e.g. Hachisu et al. 1999). Conversely, if efficient growth of the CO WD does not occur, the envelope of the secondary is dispersed in the interstellar medium, leaving behind two close WDs. The binary system has a second chance to give rise to a SNIa event, since, due to the emission of gravitational waves radiation, orbital energy is lost and the two WDs eventually merge. If the total mass of this Double Degenerate (DD) system exceeds the Chandrasekhar limit a SNIa may be produced (Iben & Tutukov 1984). While the modeling of the binary system evolution from its birth to the final explosion is subject to many rel-

* Tel: +33 1 57 27 60 51 / Fax: +33 1 57 27 60 71
Email addresses: blanc@apc.univ-paris7.fr (G. Blanc), laura.greggio@oapd.inaf.it (L. Greggio).

atively uncertain prescriptions, the nucleosynthetic product of the explosion seems more robustly assessed, and it consists of mainly Fe peak elements, and intermediate (Si group) mass elements (Iwamoto et al. 1999). The time delay between the birth of the binary system and the final explosion spans a wide range, from a few 10^7 yrs, corresponding to the nuclear evolutionary lifetime of the more massive systems, up to a Hubble time or more, especially for the DD systems born with the larger separations. As a consequence, the scaling of the SNIa rate with time will reflect not only the star formation history of the parent stellar system, but also the distribution of the delay times.

In this paper we analyze the constraints on the progenitors of CCSN, on the distribution of the delay times of SNIa, and on the cosmic history of star formation which can be derived from the measurements of the cosmic SN rates of the two kinds. Previous studies on this subject include Jorgensen et al. (1997); Sadat et al. (1998); Dahlén & Fransson (1999); Dahlen et al. (2004); Förster et al. (2006). With respect to these, we try to test the conclusions versus the choice of relevant parameters, by considering a variety of options for the distribution of the delay times and for the SFH.

The paper is organized as follows: in Sec. 2, SNR measurements are reviewed; in Sec. 3, the various theoretical ingredients hidden in the SNR evolution are dissected; in Sec. 4 we discuss the fit of the models to the observed cosmic SNIa rate in the field and in clusters, and to the observed cosmic CCSN rate. In Sec. 5 we discuss the implications of our results on the evolution of the Fe density in the universe. Conclusions are drawn in Sec. 6.

We use the concordance cosmological model $(\Omega_{M_\circ}, \Omega_{\Lambda_\circ}) = (0.3, 0.7)$, with a Hubble constant set to $\mathrm{H}_\circ = 70 h_{70}\,\mathrm{km\,s^{-1}Mpc^{-3}}$. We use the SNu or "*SuperNova Unit*", $1\,\mathrm{SNu} = 1\,\mathrm{SN}/10^{10}\mathrm{L}_{B\odot}/\mathrm{century}$.

2. Supernova rate measurements

Together with the first high-redshift supernova searches, the 1990's have seen the first type Ia rate measurement beyond the local universe (Pain et al. 1996) at $z \sim 0.4$, using for the first time a homogeneous sample of CCD discovered SNe. Other supernova searches or surveys have provided an estimate of the rate at various redshifts: EROS – Hardin et al. (2000); Blanc et al. (2004), SCP – Pain et al. (2002), SDSS – Madgwick et al. (2003), HZT – Tonry et al. (2003), Barris & Tonry (2006), GOODS – Dahlen et al. (2004); Kuznetsova et al. (2008), SNLS – Neill et al. (2006), Subaru Deep Field – Poznanski et al. (2007), STRESS – Botticella et al. (2008). Tab. 1 summarizes all the present SNIa rate measurements including the rate in the local universe derived by combining the Cappellaro et al. (1999) determinations for all galaxy kinds, for homogeneity with the high redshift measurements.

Several attempts have been made to measure the SNIa rate in galaxy clusters. This approach is interesting since the galaxy population in cluster seems rather homogeneous and old. First measurement in high redshift clusters has been made by Gal-Yam et al. (2002), with little statistics. Reiss (2000) used the *Mount Stromlo Abell Cluster SN Search* to derive a rate within clusters. The latest measurement of this kind has been published by Sharon et al. (2007), where a summary of all current SNIa rate measurements in clusters is presented.

First high-redshift measurements of the CCSN rate have been published by two teams almost simultaneously, the STRESS survey (Cappellaro et al. 2005) and the GOODS survey (Dahlen et al. 2004). The result from STRESS survey by Botticella et al. (2008) supersedes the one of Cappellaro et al. (2005). Tab. 2 summarizes these measurements. The high-redshift CCSN sample used to derive the rate is not completely based on spectroscopic confirmation, both for Cappellaro et al. (2005); Botticella et al. (2008) and Dahlen et al. (2004) measurements. Another source of uncertainty may come from the extinction within the host, since CCSN are known to occur shortly after their birth in highly dusty star formation regions of galaxies. Measurements by Cappellaro et al. (1999) are not corrected for extinction. Dahlen et al. (2004) attempted to make such a correction by simulating the host dust distribution according to the disk inclination, following the prescription by Hatano et al. (1998). Their corrected rates (as used in this paper) are a factor of ~ 2 higher than the uncorrected. We notice, however, that such a correction is still uncertain as discussed by the authors. Botticella et al. (2008) did a modeling of host galaxy extinction following the recipe of Riello & Patat (2005); their rate measurements take it into account both for SNIa and CCSN.

3. Modelization of the supernova rate evolution

The SN rate ($\mathcal{R}_{\rm SN}$) as a function of time can be modeled as the convolution of the SFH (Ψ) with the distribution function ($f_{\rm SN}$) of the delay times (τ):

$$\mathcal{R}_{\rm SN}(t) = \int_{\tau_{\rm min}}^{\min(t,\tau_{\rm max})} k_\Gamma(t-\tau)\cdot\Psi(t-\tau) f_{\rm SN}(\tau) A_{\rm SN}(t-\tau) d\tau \quad (1)$$

where t is the time elapsed since the beginning of star formation in the system under analysis; k_Γ is the number of stars per unit mass of the stellar generation with age τ; $\tau_{\rm min}$ and $\tau_{\rm max}$ bracket the range of possible delay times; $A_{\rm SN}$ is the number fraction of stars from the stellar generation born at epoch $(t-\tau)$ that end up as SN. For core-collapse events, the progenitor life-time is very short, ($\tau < 0.05$ Gyr), so that Eq. (1) can be approximated as:

$$\mathcal{R}_{\rm CC}(t) = k_\Gamma A_{\rm CC}\cdot\Psi(t) \quad (2)$$

with the SFR and number of SN per unit mass of the parent stellar generation ($k_\Gamma A_{\rm CC}$) evaluated at the current epoch. For type Ia events a very wide range of delay times is predicted from stellar evolution, with $\tau_{\rm min}$ of a few tens of Myr,

and $\tau_{\rm max}$ of the order or one Hubble time, or more. We can still introduce a little simplification to Eq. (1) by assuming that the number of SNIa from 1 $M_\odot$ stellar generation does not depend on time and write:

$$\mathcal{R}_{\rm Ia}(t) = k_\Gamma A_{\rm Ia} \cdot \int_{\tau_{\rm min}}^{\tau_{\rm max}} \Psi(t-\tau) f_{\rm Ia}(\tau) d\tau \quad (3)$$

which shows that the SNIa rate evolution depends both on the SFH and on the distribution of delay times.

Both $A_{\rm CC}$ and $A_{\rm Ia}$ can be evaluated from stellar evolution, including a choice for the IMF. However, these theoretical values depend on assumption on the mass range of the progenitors. In addition, $A_{\rm I}a$ depends on the distribution of binary separations and mass ratios, the outcome of the mass exchange phases, and of the final accretion on top of the WD. Therefore, we prefer to determine these quantities empirically from the fit of the SN rates, and compare the derived values to the theoretical expectations.

3.1. *The Star Formation History*

The SFH, $\Psi(t)$, is currently measured up to $z \sim 6$ (with some estimates up to $z \sim 10$, Bouwens et al. (2005)) from galaxy surveys, using luminosity tracers and exploiting correlations of SFH with UV, H_α, FIR luminosities (see e.g. Kennicutt (1998)). It has been pointed out that short-wavelength measurements lead to an underestimate of the SFR because of dust absorption at high-redshift. Then FIR luminosity which is less affected by the dust obscuration might be a better indicator (Chary & Elbaz 2001). Fig. 1 shows the compilation of SFR measurement by Hopkins (2004) and Hopkins & Beacom (2006), who rescale the literature data to derive a homogeneous sample, with the same cosmology, IMF and correction for absorption. Although the data points generally describe a consistent picture, there are large discrepancies at given redshift, which likely follow from the different systematics in the heterogeneous sample (see discussion in Hopkins & Beacom (2006)). As a result, several laws for $\Psi(t)$ are consistent with the data. For our exercise, we consider the following two options: Chary & Elbaz (2001) SFH – hereafter CE, a model derived from far-IR SFR measurements under the form of acceptance interval, which we implement with its average values at each redshift (middle blue curve in Fig. 1); and the function introduced by Cole et al. (2001) and used by Hopkins & Beacom (2006) to fit their SFR measurements compilation: $\rho_\star(z) = 0.7 h_{70}(a+bz)/(1+(z/c)^d)$. Our fit to the data based on a Salpeter IMF gives: $a = 0.0134, b = 0.175, c = 2.93, d = 3.01$. The two SFH mainly differ in their peak in redshift, which is $\simeq 0.8$ and 2 respectively for CE and Cole. They also correspond to two different values for the total gas mass cycled into stars, with CE being a factor 1.3 larger than Cole's.

Since $\Psi(t)$ is derived from sampling the massive stars, a large extrapolation factor is implied in the derivation of the total SFR, which depends on the assumed IMF. In addition, the conversion factor between UV luminosity and star formation rate in massive stars depends on the slope of the IMF in the high mass range. As long as this slope is similar to the Salpeter's the conversion factor does not change, and the $\Psi(t)$ derived for Salpeter IMF can be rescaled to another IMF with a different proportion of low mass stars. In our computations we adopt a Salpeter IMF.

3.2. *The Distribution of the delay times*

The distribution function of the delay times describes the proportion of early and late explosions past an instantaneous burst of star formation. Indeed, for such a case Eq. (3) becomes:

$$\mathcal{R}_{\rm Ia}(t) = k_\Gamma A_{\rm Ia} \cdot \mathcal{M}_{\rm B} \cdot f_{\rm Ia}(\tau = t) \quad (4)$$

where $\mathcal{M}_{\rm B}$ is the total gas mass turned into stars in the burst. The theoretical $f_{\rm Ia}$ function is uncertain because of various reasons: on the one hand there exist different classes of potential SNIa progenitors, on the other, the delay time distributions of each class depend on the distribution of binary parameters, and on the effect on them of the mass exchange phases which occur during the evolution of close binary systems (see Greggio 2005, for a discussion). In the literature different formulations can be found for $f_{\rm Ia}$, some stemming from stellar evolution prescriptions (e.g. Sadat et al. 1998; Yungelson & Livio 2000; Han & Podsiadlowski 2003, 2004; Greggio 2005), others from convenient analytical parametrizations (e.g. Madau et al. 1998; Mannucci et al. 2005; Scannapieco & Bildsten 2005), others from the fit of the observed time behaviour of the SNIa rate (e.g. Strolger et al. 2004). For this paper we have selected a few of these proposed distribution function of the delay times to evaluate their impact on the interpretation of the cosmic evolution of the SNIa rate, namely the Madau et al. (1998) formulation, a selection of Greggio (2005) models, and a selection of the Han & Podsiadlowski (2003, 2004) simulations. The first are parametric analytic formulae which allow the exploration of a wide range of shapes; the third is meant to illustrate the result of specific predictions from binary population synthesis.

Left panel in Fig. 2 shows examples of the Madau et al. (1998) distributions, i.e.

$$f_{\rm Ia}(\tau) \propto \int_{\max(m_{\rm Ia_{min}}, (\tau/10)^{-0.4})}^{m_{\rm Ia_{max}}} \exp\left(-\frac{\tau - t_{\rm ms}}{\tau_{\rm Madau}}\right) m^{-2.35} dm \quad (5)$$

where $t_{\rm ms} = 10/m^{2.5}$ is the main sequence lifetime (in Gyr) of a star of mass m (in $M_\odot$), and $\tau_{\rm Madau}$ is a characteristic delay time, considered as a free parameter. $m_{\rm Ia_{min}}$ and $m_{\rm Ia_{max}}$ bracket the mass range of SNIa progenitors, for which we have adopted 3 and 9 $M_\odot$ respectively. As $\tau_{\rm Madau}$ increases, the distribution of the delay times becomes wider,

still with most of the explosions occurring at early delays. For a long $\tau_{\rm Madau}$ the distribution becomes flat.

The central panel in Fig. 2 shows the selected models from Greggio (2005). These are analytic delay time distribution functions based on general arguments on the evolutionary behaviour of stars in binary systems. The different SD models, shown as dotted lines, correspond to different schemes for the derivation of the distribution of primary and secondary mass in the SNIa progenitors, and to different options for the explosion (Chandrasekhar or Sub-Chandrasekhar). All cases adopt a flat distribution of the mass ratios (i.e. $\mu = 0$). The DD models, shown as solid lines, are characterized by different assumptions about the result of the first common envelope evolution (WIDE or CLOSE systems), and different slopes for the distribution of the separations of the DD system at birth. This is described by the β parameter, whose definition is different in the CLOSE ($\beta_{\rm g}$) and WIDE DD ($\beta_{\rm a}$) schemes. Larger values of these parameters imply flatter slopes of the distribution of the delay times at late epochs. All DD models in Fig. 2 assume that the minimum mass of the secondary component in SNIa progenitor system is $\simeq 2.5$ M$_\odot$, which corresponds to a maximum nuclear delay of $\tau_{{\rm n},x} = 0.6$ Gyr. We refer the reader to the Greggio (2005) paper for a more detailed description of the parameters. All of the distribution functions in Fig. 2 exhibit an early rise, followed by a populated peak of variable width, followed by a tail of late explosions. The proportion of early-to-late epoch explosions is highly variable among the different models.

In Fig. 2 we also plot our adopted models from Han & Podsiadlowski (2003, 2004) in the right panel. The Han DD model (red), refers to double degenerate progenitors, with a standard parametrization for the common envelope evolution ($\alpha_{\rm CE} = \alpha_{\rm th} = 1, \alpha_{\rm RLOF} = 0.5$ in Han & Podsiadlowski (2003) notation). The Han SD model (green) is a single degenerate, Chandrasekhar model with initial secondary masses between ~ 2 and 3.5 M$_\odot$. These limits follow from the requirement of stability during the mass transfer from the donor to the WD, so that the latter component can reach the Chandrasekhar mass. The direct consequence of the lower limit on the secondary mass is that this SD model lacks the late delay times tail in the $f_{\rm Ia}$ function.

4. Results

In this section we explore which constraints can be derived by the analysis of the cosmic SN rate, by applying Eqs. (2) and (3). Fits of SN rate are done by a χ^2 method, providing an estimate of goodness-of-fit as a "χ^2 probability". We note that the supernova rate statistics is poissonian, which converges toward gaussian statistics for big numbers. Although most of SN rate used in this paper are based on small numbers of events, we assume that we can use the χ^2 fitting method. Systematic errors (when available), are taken into account by adding them quadratically to the statistical error. For each fit we derive a value for the $k_\Gamma A_{\rm SN}$ factor, *i.e.* the number of SN per unit mass [1] from the parent stellar population needed to account for the observed level of the rates.

The SNIa rates by Dahlen et al. (2004) have been recently re-computed by Kuznetsova et al. (2008) with a more sophisticated method. For our fit we adopt the most up-to-date values.

Similarly, for the STRESS survey, we adopt the CCSN rate in Botticella et al. (2008) which updates the Cappellaro et al. (2005) value on the basis of a larger SN sample.

4.1. *SNIa rate and SNIa progenitors*

Fig. 3 illustrates our fit with the Madau's functions. The best case is obtained with $\tau_{\rm Madau} = 1$ Gyr, corresponding to a very peaked distribution of the delay times (cf. Fig. 2), in combination with CE SFH. Cole et al. (2001)'s cosmic SFR is excluded by about 3-sigma ($\mathcal{P}(\chi^2) = 5 \cdot 10^{-3}$). Similarly, Fig. 4 shows the fit to the data with the Greggio (2005) distribution functions. The Cole et al. (2001)'s SFH do not provide a very good fit, while they all get a significant fit probability (over a few percents) when CE's SFH is adopted. Fig. 5 shows the fit based on our Han and Podsiadlowski selected models. Again the best fit is obtained in combination with CE SFH. The main difference between the two SFH is the position of maximum, $z_{\rm max} \sim 0.8$ for Chary & Elbaz (2001), and $z_{\rm max} \sim 2$ for Cole et al. (2001). We conclude that the SNIa rate data favor a maximum of SFH at late epoch in the history of the universe.

Förster et al. (2006) obtained a similar conclusion with different ingredients: the typical delay time of SNIa progenitors inferred from the cosmic evolution of their rate depends on the SFH adopted. Inspection of Fig. 4, however, shows that even for a given cosmic SFH, the model for the SNIa progenitors is not well constrained, with all models running very close to each other. Although an adopted cosmic SFH allows to solve for one most probable delay time, this does not tell much about the progenitors of SNIa, whose delay times are spread over a wide distribution.

In general, the diagnostic power of the cosmic SNIa rate is relatively weak, due to the fact that these data are averages of the SNIa rate in all galaxy types, over the SFH of the whole universe. In other words, it results from the convolution of the $f_{{\rm I}a}$ function with a wide $\Psi(t)$ function. A better way to constrain the SNIa model would consist in considering the SNIa rate evolution as function of galaxy type or in galaxy clusters, which are characterized by a relatively narrow $\Psi(t)$ (Gal-Yam et al. 2002). This is attempted in the next section.

The values obtained for the $k_\Gamma A_{\rm Ia}$ factors (where $k_\Gamma = 2.83$ M$_\odot^{-1}$ for a Salpeter IMF) from fitting the cosmic SNIa

[1] This is the mass of the stellar population at zero age, which is larger than its mass at any subsequent age because of the mass return from stars.

rate with Greggio's distributions range in $[0.45-0.55]\cdot 10^{-3}$ $M_\odot^{-1}$ and $[0.58-0.71]\cdot 10^{-3}$ $M_\odot^{-1}$ when adopting CE and Cole SFH respectively. The difference reflects the different total star formation for the two options, with CE providing more stellar mass than Cole's, so that the level of the SNIa rate is recovered in combination with a lower realization probability of the event. The fit obtained with Han distributions and CE SFH yields similar values: $k_\Gamma A_{\rm Ia} = [0.33; 0.53]\cdot 10^{-3}$ $M_\odot^{-1}$ for DD and SD models respectively. Notice that the fits obtained with Han's distributions in Fig. 5 bracket the curves obtained with Greggio's distributions. We compare these derived factors to the number of stars per unit mass of the parent stellar population with mass between 3 and 9 $M_\odot$, which is an indicative range of the mass of SNIa progenitors (Umeda et al. 1999). Since Salpeter IMF provides 0.022 $M_\odot^{-1}$ such stars, the $k_\Gamma A_{\rm Ia}$ factors require that about 2-3 % of them give rise to a SNIa event.

We notice the large discrepancy between rates measured by Barris & Tonry (2006) at $z \gtrsim 0.5$ and by others: at $z \sim 0.55$ the discrepancy with the Pain et al. (2002) measurement reaches more than 3σ. Since the Barris & Tonry (2006) measurements are not fully based on spectroscopical confirmation and do not include systematics errors, we also perform the fit excluding the 3 discrepant points. The resulting $k_\Gamma A_{\rm Ia}$ factors change for less than 20 % but the quality of fit drastically increases, 91 to 97 % for Greggio models combined with CE SFH, and 54 to 70 % for Greggio with Cole SFH. This favors Han's DD model (97 % and 74 % for CE and Cole SFH respectively), while their SD model gets a 50 % fit probability. The quality of the fits has become so close that we cannot conclude for one or the other SFH model. In this respect, we notice that rate by Dahlen et al. (2004) at $z \sim 0.8$ is similar to the Barris & Tonry (2006) value, but its redetermination by Kuznetsova et al. (2008), and the new data by Poznanski et al. (2007) favor lower SNIa rates at these redshifts.

4.2. *SNIa rate in galaxy clusters*

The galaxy population in clusters is dominated by Early Type Galaxies (ETGs), which, according to current understanding, contain mostly old stars (see Renzini 2006, for a review). This is so not only in the local universe, but at least all the way to $z \sim 1$ (Tanaka et al. 2005). Therefore, it is generally expected that the evolution of the SNIa rate in clusters of galaxies basically traces the evolution of the SNIa rate in ETGs, which closely scales as the distribution function of the delay times, as long as their SFH can be described as a short initial burst (Gal-Yam & Maoz 2004).

In a cluster, the SNIa rate in SNu, $\mathcal{R}_{\rm Ia,SNu}$, is given by the sum over the cluster members of their individual rates in SNu, $R_{\rm Ia,SNu}$, weighted by their contribution to the total B luminosity, f_B:

$$\mathcal{R}_{\rm Ia,SNu} = \sum_i R_{{\rm Ia,SNu},i}\cdot f_{B,i}. \qquad (6)$$

Both the individual rates and $f_{B,i}$ factors vary with redshift, so that in order to compute the expected trend for the rate in clusters one should specify the galaxy population in detail. On the other hand, in spite of the observed variation of the cluster galaxy population with redshift (Dressler et al. 1997; Poggianti 2006), the evolution of the bright portion of the luminosity function in clusters is consistent with that of a passively evolving model in which galaxies form their stars in a single burst at high ($z \sim 2,3$) redshift (de Propris et al. 1999). This justifies approximating the right hand side of Eq. (6) with the evolution of the rate obtained for such stellar population. By applying Eq. (4) we have:

$$\mathcal{R}_{\rm Ia,SNu}(t) \simeq k_\Gamma A_{\rm Ia}\cdot(\mathcal{M}/L_B)\cdot f_{\rm Ia}(\tau = t - t_f) \qquad (7)$$

where t is age of the universe at a given redshift, and t_f is the formation epoch of the stellar population. Thus, the SNIa rate in galaxy clusters as a function of redshift (in SNu) scales as the product of the mass-to-light ratio and the distribution function of the delay times, both of which depend on the age of the stellar population at the various redshifts. The fit of this relation to the corresponding data yields a value for the $k_\Gamma A_{\rm Ia}$ factor. Sharon et al. (2007) present the SNIa rate in clusters as a function of redshift. We plot their data in Fig. 6, together with our fits [2] obtained with a formation redshift of 3. We checked the dependence of the fit on formation redshift by adopting $z_f = 2,4$ and found it to be small. We have included in the fit the local value as measured by Cappellaro et al. (1999) for E/SO galaxies in the field. Actually, even if ellipticals in the field may be slightly younger than those in clusters (e.g. Thomas et al. 2005), the low sensitivity of our fit to the formation redshift makes the use of this local measurement reliable. If we exclude the Cappellaro et al. (1999) point from the fit, we derive a $\sim$ 40 % larger value for both $k_\Gamma A_{\rm Ia}$ and its error bar. The mass-to-light ratios as function of redshift have been derived by integrating Girardi et al. (2002) solar metallicity isochrones with a straight Salpeter IMF.

Our fit with Madau's functions shows that the data favour relatively large values of $\tau_{\rm Madau}$: the fit with $\tau_{\rm Madau} = 1$ implies a too rapid growth of the SNIa rate with redshift. This result is different from that in Maoz & Gal-Yam (2004), who, based on the same data, conclude for a relatively short $\tau_{\rm Madau}$ (< 2 Gyr for a formation redshift of 2). The different conclusion likely follows from the different approach; in particular we consider the variation of the mass to light ratio with redshift, while they do not. The decrease of M/L_B with increasing redshift counterbalances the growth of the distribution function of the delay times, resulting into a slower expected evolution of the rate in SNu with redshift.

Fig. 6 shows that due to the large error bars, no real constraint on the distribution function of the delay times

[2] The fit for Han SD model cannot be performed, since the SNIa rate from this model is zero when the population is older than 1.5 Gyr (see Fig. 2).

can be derived at present. Most of the error bar reflects the low number statistics (Sharon et al. 2007) so that future surveys will greatly improve the situation. The models in Fig. 6 illustrate the diagnostic from this kind of data: if the rapid growth of the SNIa rate with redshift is confirmed, the DD models in Greggio's formulation would be unfavoured, since they correspond to a flat behaviour of the rate at redshifts smaller than ~ 1. The steep trend exhibited by the SD Chandrasekhar models (blue and green dashed lines) mirrors the steep late epoch decline of the distribution function of the delay times for these kind of progenitors, due to the requirement that the WD reaches the Chandrasekhar mass by accreting the envelope of a progressively less massive companion (see e.g. Greggio 2005, for more details).

The derived values for the number of SNIa from 1 $M_\odot$ stellar population are affected by a larger uncertainty with respect to what we get from fitting the rate in the field. Averaging over all Greggio's models we get $k_\Gamma A_{\rm Ia} = 1.7 \cdot 10^{-3}$ $M_\odot^{-1}$, not far from those obtained in the previous section. We acknowledge a difference of a factor of ~ 3, favouring events in clusters, at a $\sim 2\ \sigma$ level. Given the different ingredients used in the two computations, assumptions on the global SFH and age distribution, and the uncertainty on the observed rates, we regard this result as encouraging, although the discrepancy needs further investigation.

An independent constraint on the $k_\Gamma A_{\rm Ia}$ factor can be derived by considering the total Fe budget of galaxy clusters. Assuming that every SNIa event ejects an average mass $m_{\rm Fe}$ of Fe, their contribution to the Fe Mass-to-Light ratio is:

$$\frac{M_{\rm Fe,Ia}}{L_B} = m_{\rm Fe} \cdot k_\Gamma A_{\rm Ia} \cdot \frac{M}{L_B} \tag{8}$$

where M/L_B is the ratio between the total gas mass turned into stars and the current B band luminosity of the typical elliptical in the cluster. For a Salpeter IMF, $M/L_B \simeq 13.5\ M_\odot \cdot L_\odot^{-1}$ at an age of 11.4 Gyr, corresponding to a formation redshift of 3. The total Fe mass to light ratio in clusters is ~ 0.02 (e.g. De Grandi et al. 2004); $\sim$ half of which is contributed from SNIa (see Sect. 5, also Greggio 2008, in preparation). Adopting $m_{\rm Fe} = 0.75\ M_\odot$ (Iwamoto et al. 1999, summing the ejected masses of ^{54}Fe and ^{56}Fe), we get $k_\Gamma A_{\rm Ia} \sim 10^{-3}\ M_\odot^{-1}$. We conclude that the three independent estimates of the $k_\Gamma A_{\rm Ia}$ agree within a factor of 2. The uncertainties currently affecting each of them prevents a more accurate determination.

4.3. *CCSN progenitor masses from CCSN rate*

Due to the short lifetime of their progenitors, in a stellar system the CCSN rate is directly proportional to the current SFR (Eq. 2), with:

$$k_\Gamma A_{\rm CC} = \frac{\int_{m_{\rm CC_{min}}}^{m_{\rm CC_{max}}} \Phi(m) dm}{\int_{m_{\star_{\rm min}}}^{m_{\star_{\rm max}}} m\Phi(m) dm} \tag{9}$$

where Φ is the IMF by number, $[m_{\star_{\rm min}}, m_{\star_{\rm max}}]$ is the whole stellar mass range and $m_{\rm CC_{min}}$ and $m_{\rm CC_{max}}$ are respectively the minimum and maximum stellar mass leading to a CCSN.

For a Salpeter IMF between 0.1 and 120 $M_\odot$:

$$k_\Gamma A_{\rm CC} = 0.126 \cdot (m_{\rm CC_{min}}^{-1.35} - m_{\rm CC_{max}}^{-1.35}). \tag{10}$$

By fitting Eq. (2) to the redshift trend of the CCSN rate with the two SFH laws described in Sec. 3.1 we obtain the related values of the constant $k_\Gamma A_{CC}$. Although the scaling of the SFH to the CCSN rate depends on the IMF, we only consider Salpeter IMF because this has been adopted for the derivation of the SFH laws. The fitting values of $k_\Gamma A_{CC}$ are reported in Fig. 7, giving similar values for CE and Cole SFH. For a given SFH we get a bijective relationship between $m_{\rm CC_{min}}$ and $m_{\rm CC_{max}}$, which is very sensitive to $k_\Gamma A_{CC}$, as plotted in Fig. 8.

The minimum mass $m_{\rm CC_{min}}$ is actually set by the heaviest star that produces a white dwarf, which can vary from 6 $M_\odot$ to 11 $M_\odot$ according to Heger et al. (2003). They used 9 $M_\odot$ as an average value. It is supported by the observations of SNII events: the lowest SNII progenitor mass known so far has been derived from the type II-P event SN 2003gd as 8^{+4}_{-2} $M_\odot$ (Smartt et al. 2004; Hendry et al. 2005), though careful modeling of the observations favors a progenitor mass closer to the upper limit of this range (Hendry et al. 2005). The maximum mass $m_{\rm CC_{max}}$ is much less constrained, but should be around ~ 40 $M_\odot$, or less. The highest main sequence masses that have been derived for CCSN event are for some type Ic connected with a hypernova event, with $m_{\rm CC_{max}} \gtrsim 40$ $M_\odot$. This kind of SN is of course included in the generic class of "CCSN event" for which the rate history has been measured. For instance the type Ic SN 2003lw has a progenitor with a mass within $[40 - 50\ M_\odot]$ (Mazzali et al. 2006). Within the type II-P SNe class, SN 2003Z has the highest "observed" mass with $m_{\rm CC_{max}} = 36.5 \pm 4.9$ $M_\odot$ (Pastorello 2003; Zampieri et al. 2003).

Fig. 8 shows that the observed and theoretical $m_{\rm CC_{min}}$ and $m_{\rm CC_{max}}$ are only compatible with the high side of the 1-σ error interval of $k_\Gamma A_{CC}$ for both CE and Cole SFH. The favored $m_{\rm CC_{min}}$ is $m_{\rm CC_{min}} \gtrsim 10$ $M_\odot$ to account for the observed $m_{\rm CC_{max}}$. But since CCSNe explode in star forming regions, a fraction of the events is likely to escape detection, so that the rate in Fig. 7 would be a lower limit to the real CCSN rate (see sec. 2). In this case, the fit with the SFH would lead to a larger value for $k_\Gamma A_{\rm CC}$, which could accommodate a wider range of CCSN progenitor's masses.

5. The released iron density evolution

The iron in the Universe is produced or released in the ISM by supernovae. Knowing the supernova rate history and the distribution of produced iron, we can estimate the evolution of the iron density with redshift. As a function of cosmic time, t, it is generally given by:

$$\rho_{\rm Fe}(t) = \int_{t_{\rm re}}^{t} \mathcal{M}_{\rm Fe}(t') \cdot \mathcal{R}_{\rm SN}(t') dt' \qquad (11)$$

where $\mathcal{M}_{\rm Fe}$ is the distribution function of iron mass released per event and $t_{\rm re}$ is the epoch of reionization corresponding to the first stars, and then the first SNe, and first iron released in the ISM.

5.1. *From type Ia SNe*

A SNIa releases in the interstellar medium (ISM), on average, 0.5 $M_\odot$ of ^{56}Ni (that becomes of ^{56}Fe after radioactive decay). During the explosion others isotopes of iron are produced, ^{54}Fe, ^{57}Fe and ^{58}Fe. The present approach is sensitive only to the "observable" iron which powers the light curve of SNIa, that is ^{56}Fe. Then we expect to miss 10 % to 15 % of iron according to delayed detonation nucleosynthesis models (Iwamoto et al. 1999); for 3-dimensional pure deflagration models, the proportion of iron isotopes other than ^{56}Fe varies from 15 % to 25 % (Travaglio et al. 2004). To take into account all iron, we assume that ^{56}Fe represents 85 % of all iron released by SNIa in the ISM. Then, in Eq. (11) the iron distribution is given by $\mathcal{M}_{\rm Fe} = 1.18\ \mathcal{M}_{^{56}{\rm Fe}} = 1.18\ \mathcal{M}_{^{56}{\rm Ni}}$, assuming that this ratio does not evolves with cosmic time [3] .

The distribution of released ^{56}Ni mass is taken from Leibundgut (2000), Mazzali et al. (2000) and Stritzinger et al. (2006); it is plotted on Fig. 9. The averaged ^{56}Ni mass as derived from observations, 0.5 $M_\odot$ per event, lies between the prediction of DD models (0.6 $M_\odot$ to 0.8 $M_\odot$, Iwamoto et al. (1999)) and predictions of pure 3-dimensions deflagration models (0.24 $M_\odot$ to 0.44 $M_\odot$, Travaglio et al. (2004)).

To render the SNIa rate measurement and integrate it easily, we fit it by an exponential between $z = 0$ and 0.59, and by a straight line for $z > 0.59$ as shown on Fig. 10. Eq. (11) is integrated by a Monte-Carlo method in order to keep the observed shape of the nickel distribution, under the assumption that the distribution of ^{56}Ni as shown on Fig. 9 is representative and independent of cosmic time. Beside the *ad hoc* shape for the SNIa rate, we use the best model fitting the rate evolution, that is the Greggio SD-SCh distribution convolved with the CE SFH (Fig. 4). The result is plotted on Fig. 10.

Since the model produces SNe Ia at redshift larger than ~ 2, for this case we get a larger amount of integrated iron, with respect to the *ad hoc* fit. Still, the difference only amounts to a factor of 1.2 at the present epoch. So SNe Ia in the distant universe have little influence on the total iron produced.

[3] Actually this ratio probably evolves with redshift since Travaglio et al. (2005) found an anticorrelation of $\mathcal{M}_{^{56}{\rm Fe}}/\mathcal{M}_{\rm Fe}$ with metallicity, going from 0.93 at 0.1 $Z_\odot$, to 0.83 at $Z_\odot$ and 0.70 at 3 $Z_\odot$. But such a study is beyond the scope of this paper.

5.2. *From CCSNe*

Like for SNIa, only ^{56}Ni powers the light curve of CCSN, by radioactive decay to ^{56}Fe. According to Iwamoto et al. (1999) a typical CCSN ejects 93 % of the total iron as ^{56}Fe; thus in our total computation, we take $\mathcal{M}_{\rm Fe} = 1.08\ \mathcal{M}_{^{56}{\rm Fe}} = 1.08\ \mathcal{M}_{^{56}{\rm Ni}}$ in Eq. (11).

According to Zampieri et al. (2003) and Hamuy (2003) the ^{56}Ni mass released by SNII is distributed as shown in Fig. 9, based on 29 SNe II. The average Ni mass is 0.066 $M_\odot$. This distribution covers more than two orders of magnitudes, while the distribution of Ni produced by SNIa spreads less than one order of magnitude. Eq. (11) is integrated over this distribution by a Monte-Carlo method, setting the redshift of the first stars to 20 (Fuller & Couchman 2000). The CCSN rate is modeled by two SFH models as previously discussed. They are plotted on Fig. 11, together with the results of the integration. The two SFH models, once calibrated on the observed rates, produce very close Fe production curves.

5.3. *Total*

Fig. 12 shows the total density of iron produced, sum of the contribution of SNIa and of CCSN. It is interesting to note that today's iron density comes from half-part of SNIa (Fig. 10) and half-part of CCSN (Fig. 11). Indeed, on average one CCSN releases 10 times less Fe than one SNIa. However, the CCSN production per unit gas mass transformed into stars is about 10 times that of SNIa production, as result from the ratio $k_\Gamma A_{\rm CC}/k_\Gamma A_{\rm Ia} \sim 7.5$. We remark that the evolution of the iron density does not depend strongly on the SFH model. Calura & Matteucci (2006) present models of cosmic metal production based on chemo-photometric models of the evolution of dwarf galaxies and spheroids in the universe. The models detail the evolution of various chemical species in different phases (ISM, IGM, Stars), and, in particular, that of the total Fe density. Fig. 12 shows as blue lines the predictions of Calura & Matteucci models for two kinds of galaxies, irregulars and spheroids, and their sum. Since the contribution of disks is missing, we cannot compare directly the Calura and Matteucci predictions (solid blue line) with our empirical curve. However, in Calura & Matteucci (2004) the iron production rate by disks becomes important only at relatively low redshift ($z \lesssim 1.2$), and at zero redshift the contribution of disks is ~ 0.6 that of ellipticals. We may then extrapolate the results of Calura & Matteucci (2006) into a total expected Fe production in the Universe of $8 \cdot 10^5$ $M_\odot$ Mpc^{-3}. This is in excellent agreement with our estimate, which is $\rho_{\rm Fe} = (8.5 \pm 0.9) \cdot 10^5$ $M_\odot$ Mpc^{-3}, as averaged from our various estimates. We also expect that the corrected curve for the total Fe in Calura and Matteucci's models is similar to what plotted in Fig. 12 for redshift in excess of ~ 1.2, so that also in the models a large fraction of Fe in the universe is produced at $z \lesssim 1$. Given the completely differ-

ent approaches for determining the cosmic increase of total Fe density, we consider the models and our empirical estimate in very good agreement. Our total current Fe density is also in excellent agreement with the value of $\rho_{\rm Fe} = 8.6 \cdot 10^5$ M$_\odot$ Mpc^{-3} by Fukugita & Peebles (2004).

We label the right axis in Fig. 12 with the Fe abundance relative to solar, having considered $Z_{\rm Fe} = \rho_{\rm Fe}/\rho_B$, where $\rho_B = \rho_\circ \cdot \Omega_B$, $\rho_\circ = 1.36 \cdot 10^{11}\ h_{70}^2 {\rm M}_\odot {\rm Mpc}^{-3}$ is the critical density of the universe and Ω_B is the density of baryon ($\Omega_B = 0.049 \pm 0.002\ h_{70}^{-2}$, see Spergel et al. 2003), which gives: $Z_{\rm Fe} = (1.28 \pm 0.14) \cdot 10^{-4}$. Adopting the solar Fe abundance by Grevesse & Sauval (1998) $Z_{\rm Fe,\odot} = (1.3 \pm 0.1) \cdot 10^{-3}$, we obtain an average Fe abundance of the universe at zero redshift of $Z_{\rm Fe} = (0.10 \pm 0.01)\ Z_{\rm Fe,\odot}$, which is a factor of $\sim$ 3-4 lower than the Fe abundance in clusters of galaxies (e.g. Renzini 2004).

Does this mean that the stellar production of Fe is different in clusters from that in the field? To answer this question we consider the ratio between the Fe and the stellar density $\eta_{\rm Fe} = \rho_{\rm Fe}/\rho_*$. In clusters: $\eta_{\rm Fe,cl} = Z_{\rm Fe,ICM} \cdot M_{\rm ICM}/M_* + Z_{\rm Fe,*} \simeq 3.3\ Z_{\rm Fe,\odot}$ having adopted $M_*/M_{\rm ICM} = 0.13$ (Ettori 2007), $Z_{\rm Fe,ICM} = 0.3 Z_\odot$ (Tamura et al. 2004), and a solar iron abundance for the stellar component. By integrating our SFH and correcting for the mass return from SNe and stellar winds [4], we find a current $\rho_* = (8.2 \pm 4.1) \cdot 10^8\ h_{70} {\rm M}_\odot \cdot {\rm Mpc}^{-3}$, which gives $\eta_{\rm Fe} = (0.8 \pm 0.4) \cdot\ Z_{\rm Fe,\odot}$ a factor $\sim$ 4 lower than in clusters. However, while these estimates of $\eta_{\rm Fe,cl}$ and of the Fe density in the field do not depend on the IMF, the stellar density in the field does. A more realistic IMF, with a turn-over at the low mass end, implies a lower stellar density for the same amount of UV photons. For example, the mass fraction in stars more massive than 1 M$_\odot$ is 0.61 and 0.39 for Chabrier (Chabrier 2005) and Salpeter IMFs respectively; the mass fraction returned to the medium from stellar winds and SNe is $\sim$ 0.45 and 0.28 for the two IMFs. Therefore, for a Chabrier IMF, the current stellar mass density becomes $\rho_*^{\rm Cha} = (4 \pm 2) \cdot 10^8$ M$_\odot$Mpc^{-3}, to yield $\eta_{\rm Fe^{Cha}} = (1.6 \pm 0.8)\ Z_{\rm Fe,\odot}$, close to the value in clusters. In addition, the rate of CCSN may be affected by a more severe incompleteness than adopted in the values in Tab. 2, particularly at high redshift, where some events could occur in heavily obscured regions (Mannucci et al. 2003). We conclude that the Fe production from stars in the field and in clusters can be brought into agreement, if the IMF has a turn over at the low mass end. The different abundance, then, stems from a different efficiency of baryon conversion into stars $\rho_*^{\rm Cha}/\rho_B$, which adopting the figures above, is ~ 0.12 in clusters and ~ 0.06 in the field.

6. Conclusions

In this paper we have investigated on the constraints which can be derived from the cosmic trend of the SN rates on the SFH, on the distribution of the delay times of SNIa progenitors and on the mass range on the CCSN progenitors. In addition, we have determined the local Fe abundance as resulting from the integration of the observed SN rates. Our results can be summarized as follows.

The observed cosmic evolution of the SNIa rate has been fit by adopting two laws for the SFH which bracket most of the observational data, namely Chary & Elbaz (2001) and Cole et al. (2001), in combination with various distribution functions of the delay times: Madau et al. (1998) models, a selection of Greggio (2005) models, and a selection of models by Han & Podsiadlowski (2003, 2004). We find that, while, within the error, it is hard to distinguish among the possible progenitor models, the fits are fairly sensitive to the adopted SFH (see also Oda et al. 2008). The increase of the SNIa rate with redshift is better reproduced with CE rather than Cole SFH. However if rate measurements by Barris & Tonry (2006) were systematically too high, the two SFH would be rather equivalent in fitting the SNIa rate data. The inability of the cosmic SNIa rate to constrain the progenitor model is related to its being an average over a galaxy population which spans a wide range of properties. Measurements of the SNIa rate in different kinds of galaxies would help us to relate the observed rate, and its redshift evolution, to the parent stellar population, in turn providing better constraints on the shape of the distribution function of the delay times.

As an attempt in this direction, we have considered the redshift evolution of the SNIa rate in galaxy clusters, assumed to harbor mainly old stellar populations. Due to the large error bars affecting the current measurements, all SNIa progenitor models provide acceptable fits. Madau's models with $\tau_{\rm Madau}$ shorter than $\sim$ 1 Gyr are however excluded. Among Greggio's models, the SD family seems favoured, but we emphasize that the error bars on the data are currently too large to draw any conclusion.

The fit to the cosmic SNIa rate and to the rate in clusters provides the number of Ia events per unit mass of the parent stellar population ($k_\Gamma A_{\rm Ia}$) which is needed to explain the observed level of the rate. The field cosmic rate and the rate in clusters indicate similar (albeit non equal) values for this constant. On the average we conclude that in both field and cluster galaxies we have $\sim$ 1 SNIa explosion every 1000 M$_\odot$ of stars in the parent population, corresponding to $\sim$ a 5 % probability of the SNIa channel, if the primaries in the binary progenitors have masses in the range 3 to 9 M$_\odot$ (for a Salpeter IMF).

The redshift evolution of the rate of CCSN is compatible with both CE and Cole SFH. The favored progenitor minimum mass is $\gtrsim 10$ M$_\odot$, even if some incompleteness in the observed CCSN rate could accommodate a (somewhat) lower CCSN's progenitor masses.

The convolution of the observed cosmic SN rates with their ejected Fe mass allows us to compute the Fe density of the universe at zero redshift. We find $\rho_{\rm Fe} = (8.8 \pm 0.9) \cdot 10^5$ M$_\odot$ Mpc^{-3}, in very good agreement with Fukugita & Peebles (2004) and Calura & Matteucci

[4] for a Salpeter IMF the correction factor amounts to 0.72 (e.g. Cole et al. 2001)

(2006). The corresponding Fe abundance in the local universe is 0.1 $Z_{\mathrm{Fe},\odot}$, which is a factor of ~ 3 lower than the Fe abundance in massive clusters. We show that, if the IMF has a turn over at the low mass end, this difference does not imply a different efficiency of Fe production from stars in the two environments, but rather it reflects a different efficiency of baryon conversion to stars.

Acknowledgments

We thank Andrew Hopkins for kindly providing his updated compilation of SFR measurements; Philipp Podsiadlowski and Zhanwen Han for useful discussions and for providing ascii forms of their SNIa delay time distribution models; Francesco Calura for quickly providing of his iron density evolution model in ascii form; Maria Teresa Botticella for providing her results on the SN rate before publication. We also thank Alvio Renzini and Enrico Cappellaro for interesting discussions. This work has been partly supported by the European Community's Human Potential Program under contract HPRN-CT-2002-00303, *The Physics of Type Ia Supernovae*.

References

Barris, B. J. & Tonry, J. L. 2006, ApJ, 637, 427
Blanc, G., Afonso, C., Alard, C., et al. 2004, A&A, 423, 881
Botticella, M. T., Riello, M., Cappellaro, E., et al. 2008, A&A, 479, 49
Bouwens, R. J., Illingworth, G. D., Thompson, R. I., & Franx, M. 2005, ApJ, 624, L5
Calura, F. & Matteucci, F. 2004, MNRAS, 350, 351
Calura, F. & Matteucci, F. 2006, MNRAS, 369, 465
Cappellaro, E., Evans, R., & Turatto, M. 1999, A&A, 351, 459
Cappellaro, E., Riello, M., Altavilla, G., et al. 2005, A&A, 430, 83
Chabrier, G. 2005, in ASSL Vol. 327: The Initial Mass Function 50 Years Later, ed. E. Corbelli, F. Palla, & H. Zinnecker, 41–+
Chary, R. & Elbaz, D. 2001, ApJ, 556, 562
Cole, S., Norberg, P., Baugh, C. M., et al. 2001, MNRAS, 326, 255
Dahlén, T. & Fransson, C. 1999, A&A, 350, 349
Dahlen, T., Strolger, L., Riess, A. G., et al. 2004, ApJ, 613, 189
De Grandi, S., Ettori, S., Longhetti, M., & Molendi, S. 2004, A&A, 419, 7
de Propris, R., Stanford, S. A., Eisenhardt, P. R., Dickinson, M., & Elston, R. 1999, AJ, 118, 719
Dressler, A., Oemler, A. J., Couch, W. J., et al. 1997, ApJ, 490, 577
Ettori, S. 2007, in Heating versus Cooling in Galaxies and Clusters of Galaxies, Eso Astrophysics Symposia, Volume . ISBN 978-3-540-73483-3. Springer-Verlag Berlin Heidelberg, 2007, p. 291, ed. H. Böhringer, G. W. Pratt, A. Finoguenov, & P. Schuecker, 291–+
Förster, F., Wolf, C., Podsiadlowski, P., & Han, Z. 2006, MNRAS, 368, 1893
Fukugita, M. & Peebles, P. J. E. 2004, ApJ, 616, 643
Fuller, T. M. & Couchman, H. M. P. 2000, ApJ, 544, 6
Gal-Yam, A. & Maoz, D. 2004, MNRAS, 347, 942
Gal-Yam, A., Maoz, D., & Sharon, K. 2002, MNRAS, 332, 37
Girardi, L., Bertelli, G., Bressan, A., et al. 2002, A&A, 391, 195
Greggio, L. 2005, A&A, 441, 1055
Grevesse, N. & Sauval, A. J. 1998, Space Science Reviews, 85, 161
Hachisu, I., Kato, M., Nomoto, K., & Umeda, H. 1999, ApJ, 519, 314
Hamuy, M. 2003, ApJ, 582, 905
Han, Z. & Podsiadlowski, P. 2003, in IAU Symposium, 109
Han, Z. & Podsiadlowski, P. 2004, MNRAS, 350, 1301
Hardin, D., Afonso, C., Alard, C., et al. 2000, A&A, 362, 419
Hatano, K., Branch, D., & Deaton, J. 1998, ApJ, 502, 177
Heger, A., Fryer, C. L., Woosley, S. E., Langer, N., & Hartmann, D. H. 2003, ApJ, 591, 288
Hendry, M. A., Smartt, S. J., Maund, J. R., et al. 2005, MNRAS, 359, 906
Hopkins, A. M. 2004, ApJ, 615, 209
Hopkins, A. M. & Beacom, J. F. 2006, ApJ, 651, 142
Iben, I., J. & Tutukov, A. V. 1984, ApJS, 54, 335
Ilbert, O., Tresse, L., Zucca, E., et al. 2005, A&A, 439, 863
Iwamoto, K., Brachwitz, F., Nomoto, K., et al. 1999, ApJS, 125, 439
Janka, H.-T., Langanke, K., Marek, A., Martínez-Pinedo, G., & Müller, B. 2007, Phys. Rep., 442, 38
Jorgensen, H. E., Lipunov, V. M., Panchenko, I. E., Postnov, K. A., & Prokhorov, M. E. 1997, ApJ, 486, 110
Kennicutt, Robert C., J. 1998, ARA&A, 36, 189
Kuznetsova, N., Barbary, K., Connolly, B., et al. 2008, ApJ, 673, 981
Leibundgut, B. 2000, A&A Rev., 10, 179
Madau, P., della Valle, M., & Panagia, N. 1998, MNRAS, 297, 17
Madgwick, D. S., Hewett, P. C., Mortlock, D. J., & Wang, L. 2003, ApJ, 599, L33
Mannucci, F., Della Valle, M., Panagia, N., et al. 2005, A&A, 433, 807
Mannucci, F., Maiolino, R., Cresci, G., et al. 2003, A&A, 401, 519
Maoz, D. & Gal-Yam, A. 2004, MNRAS, 347, 951
Mazzali, P. A., Cappellaro, E., Turatto, M., et al. 2000, Memorie della Societa Astronomica Italiana, 71, 411
Mazzali, P. A., Deng, J., Pian, E., et al. 2006, ApJ, 645, 1323
Neill, J. D., Sullivan, M., Balam, D., et al. 2006, AJ, 132, 1126
Oda, T., Totani, T., Yasuda, N., et al. 2008, ArXiv e-prints,

801
Pain, R., Fabbro, S., Sullivan, M., et al. 2002, ApJ, 577, 120, (The Supernova Cosmology Project)
Pain, R., Hook, I. M., Deustua, S., et al. 1996, ApJ, 473, 356, (The Supernova Cosmology Project)
Pastorello, A. 2003, PhD thesis, Università degli studi di Padova
Poggianti, B. M. 2006, in The Many Scales in the Universe: JENAM 2004 Astrophysics Reviews, ed. J. C. Del Toro Iniesta, E. J. Alfaro, J. G. Gorgas, E. Salvador-Sole, & H. Butcher, 71–+
Poznanski, D., Maoz, D., Yasuda, N., et al. 2007, MNRAS, 382, 1169
Reiss, D. 2000, PhD thesis, University of Washington
Renzini, A. 2004, in Clusters of Galaxies: Probes of Cosmological Structure and Galaxy Evolution, ed. J. S. Mulchaey, A. Dressler, & A. Oemler, 260–+
Renzini, A. 2006, ARA&A, 44, 141
Riello, M. & Patat, F. 2005, MNRAS, 362, 671
Sadat, R., Blanchard, A., Guiderdoni, B., & Silk, J. 1998, A&A, 331, L69
Scannapieco, E. & Bildsten, L. 2005, ApJ, 629, L85
Sharon, K., Gal-Yam, A., Maoz, D., Filippenko, A. V., & Guhathakurta, P. 2007, ApJ, 660, 1165
Smartt, S. J., Maund, J. R., Hendry, M. A., et al. 2004, Science, 303, 499
Spergel, D. N., Verde, L., Peiris, H. V., et al. 2003, ApJS, 148, 175
Stritzinger, M., Mazzali, P. A., Sollerman, J., & Benetti, S. 2006, A&A, 460, 793
Strolger, L., Riess, A. G., Dahlen, T., et al. 2004, ApJ, 613, 200
Tamura, T., Kaastra, J. S., den Herder, J. W. A., Bleeker, J. A. M., & Peterson, J. R. 2004, A&A, 420, 135
Tanaka, M., Kodama, T., Arimoto, N., et al. 2005, MNRAS, 362, 268
Thomas, D., Maraston, C., Bender, R., & Mendes de Oliveira, C. 2005, ApJ, 621, 673
Tonry, J. L., Schmidt, B. P., Barris, B., et al. 2003, ApJ, 594, 1
Travaglio, C., Hillebrandt, W., & Reinecke, M. 2005, A&A, 443, 1007
Travaglio, C., Hillebrandt, W., Reinecke, M., & Thielemann, F.-K. 2004, A&A, 425, 1029
Woosley, S. E., Heger, A., & Weaver, T. A. 2002, Reviews of Modern Physics, 74, 1015
Woosley, S. E. & Weaver, T. A. 1986, ARA&A, 24, 205
Yungelson, L. R. & Livio, M. 2000, ApJ, 528, 108
Zampieri, L., Ramina, M., & Pastorello, A. 2003, astro-ph/0310057

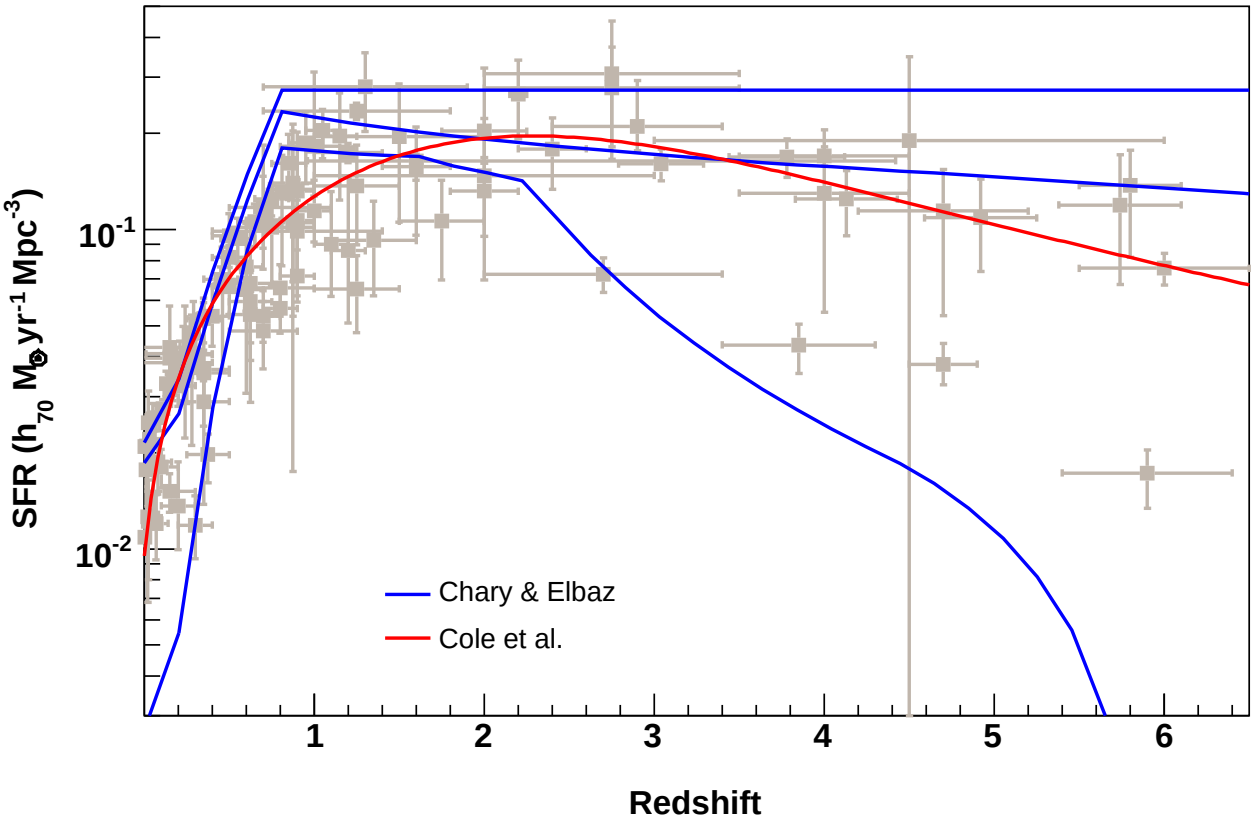

Fig. 1. Measured cosmic SFR as compiled by Hopkins (2004) and Hopkins & Beacom (2006). Models are from Chary & Elbaz (2001), extrapolated for $z > 4.5$ and Cole et al. (2001).

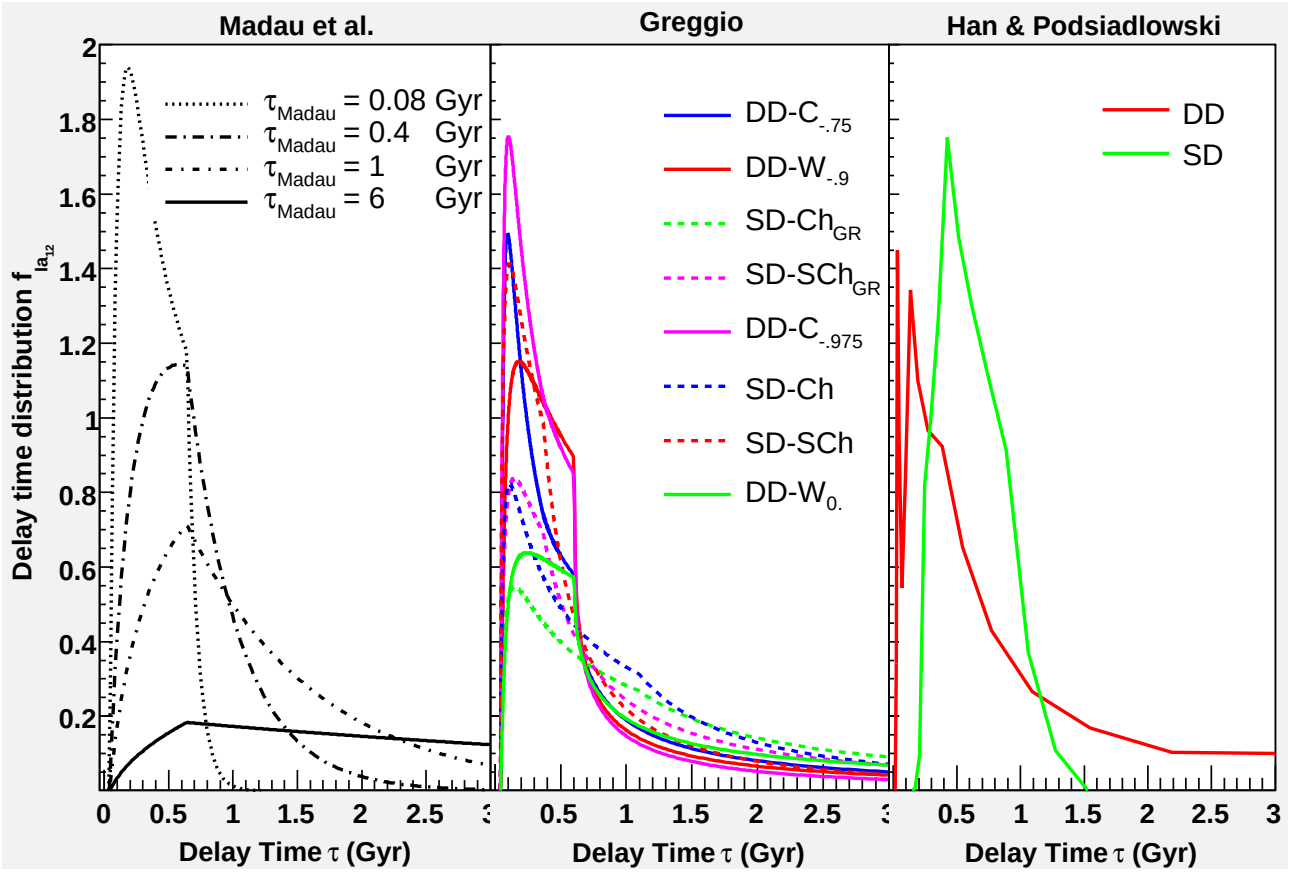

Fig. 2. Delay time distributions used: Madau et al. (left), Greggio (middle) and Han and Podsiadlowski (right). They are all normalized over the range 0-12 Gyr.

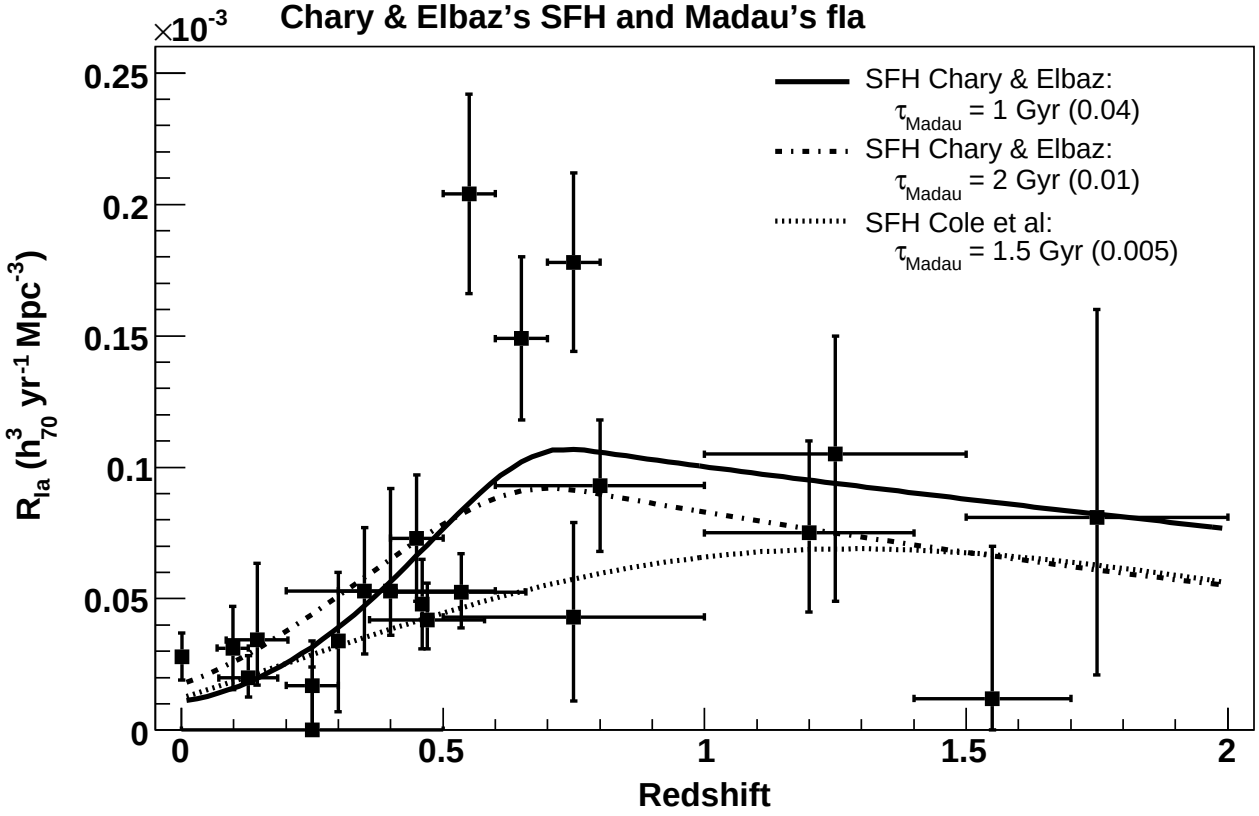

Fig. 3. SNIa rate measurements fitted with Madau's delay time distribution and both CE and Cole SFH. The value of the fitted Madau's τ parameter (here $\tau_{\rm Madau}$) is indicated. χ^2 fit probabilities are shown in parenthesis: best fits are $\tau_{\rm Madau} = 1$ Gyr for CE SFH, and $\tau_{\rm Madau} = 1.5$ Gyr for Cole SFH.

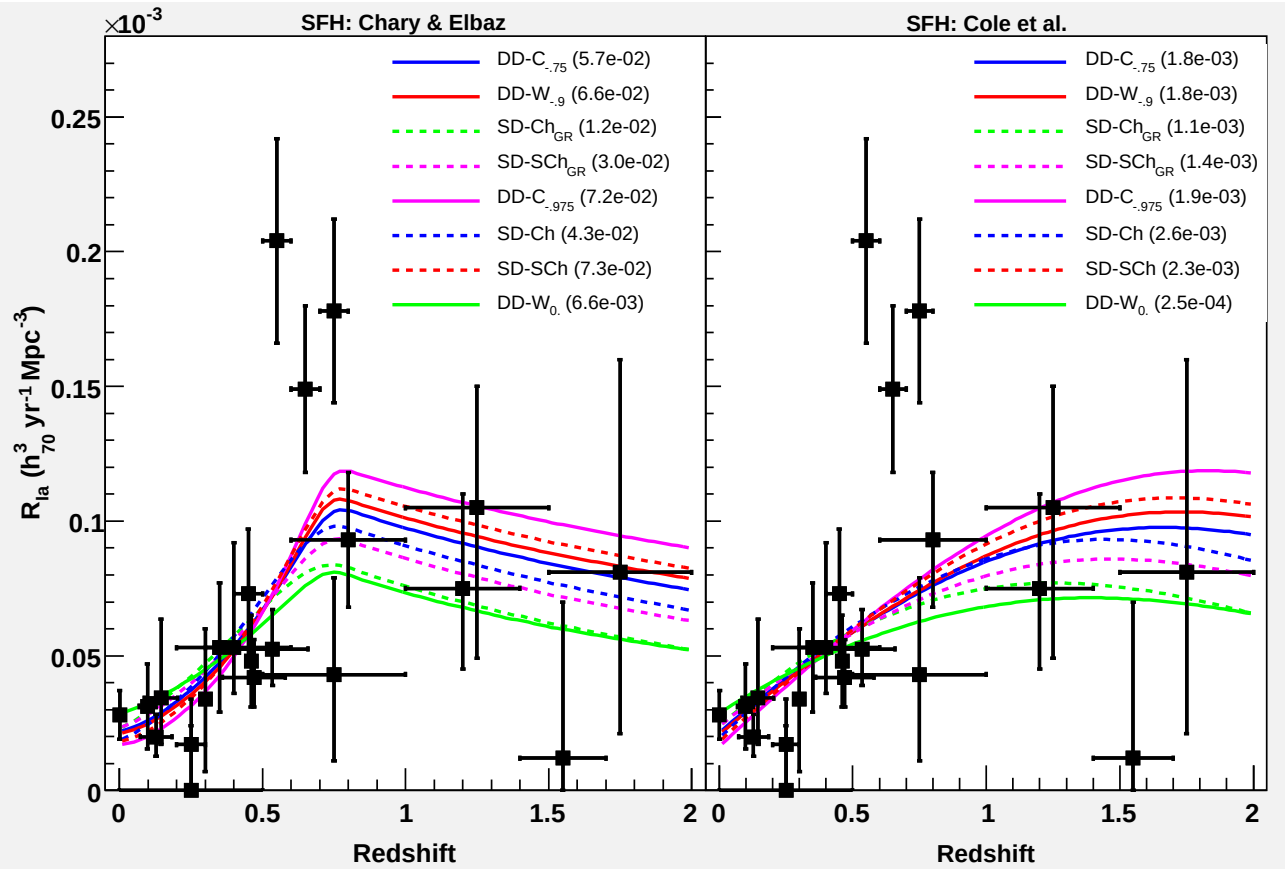

Fig. 4. SNIa rate measurements fitted with Greggio's delay time distribution and SFH from CE (left) and Cole et al. (right). χ^2 fit probabilities are shown in parenthesis.

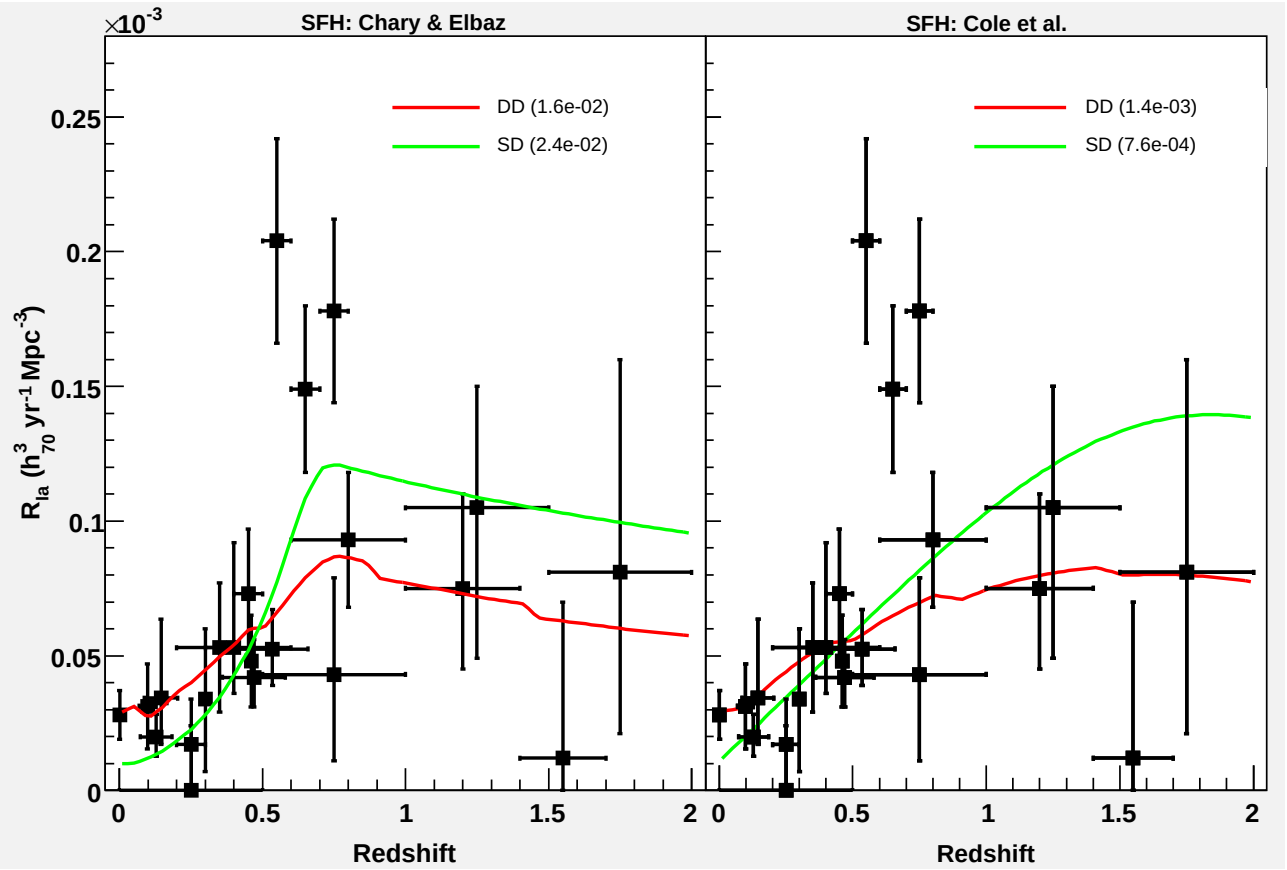

Fig. 5. SNIa rate measurements fitted with Han and Podsiadlowski's delay time distribution and SFH from CE (left) and Cole et al. (right). χ^2 fit probabilities are shown in parenthesis.

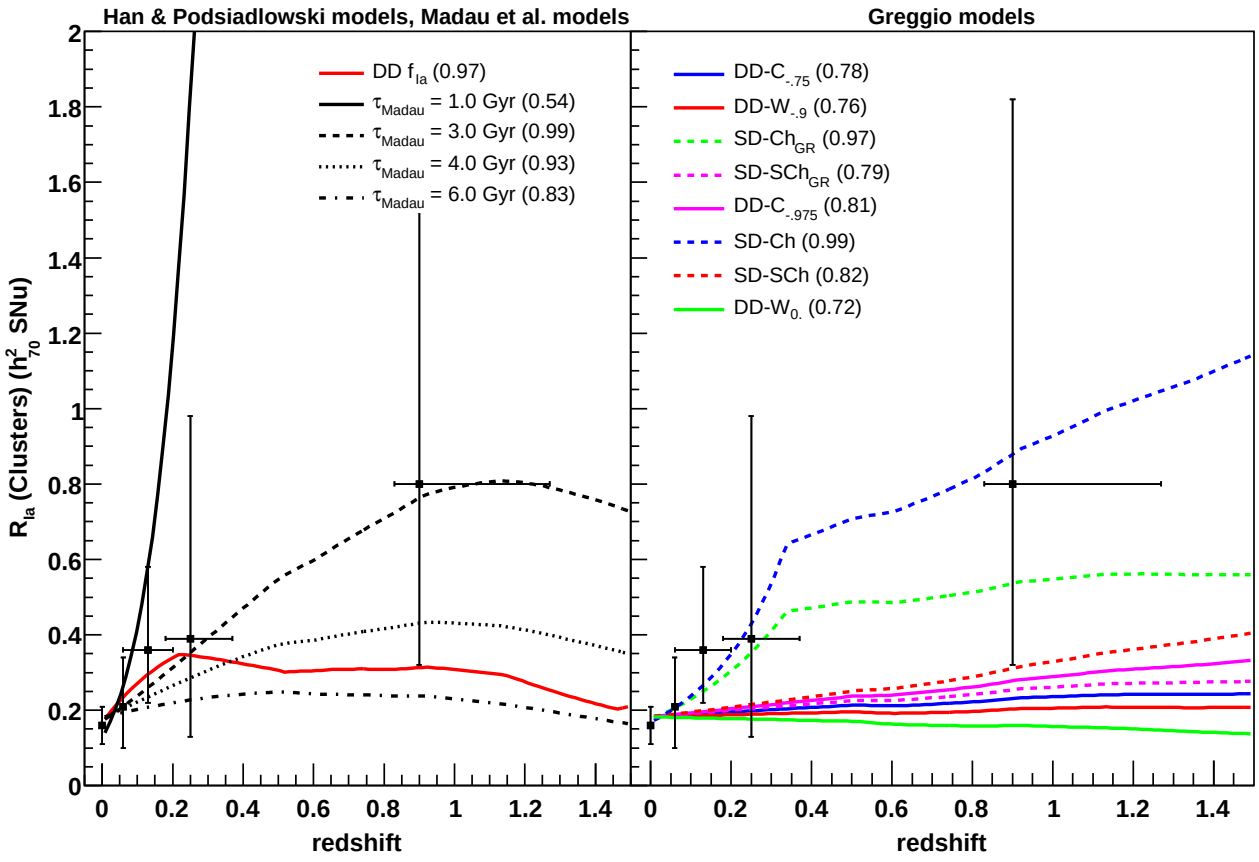

Fig. 6. SNIa rate measurements in clusters fitted with Han's and Madau's models (left), and Greggio's delay time distributions for an epoch of ellipticals formation of $z_f = 3$. χ^2 fit probabilities are shown in parenthesis. Data are from Cappellaro et al. (1999) at $z \sim 0$, Reiss (2000) at $z = 0.11$, Sharon et al. (2007) at $z = 0.13$ and Gal-Yam et al. (2002) at $z = 0.25$ and $z = 0.90$.

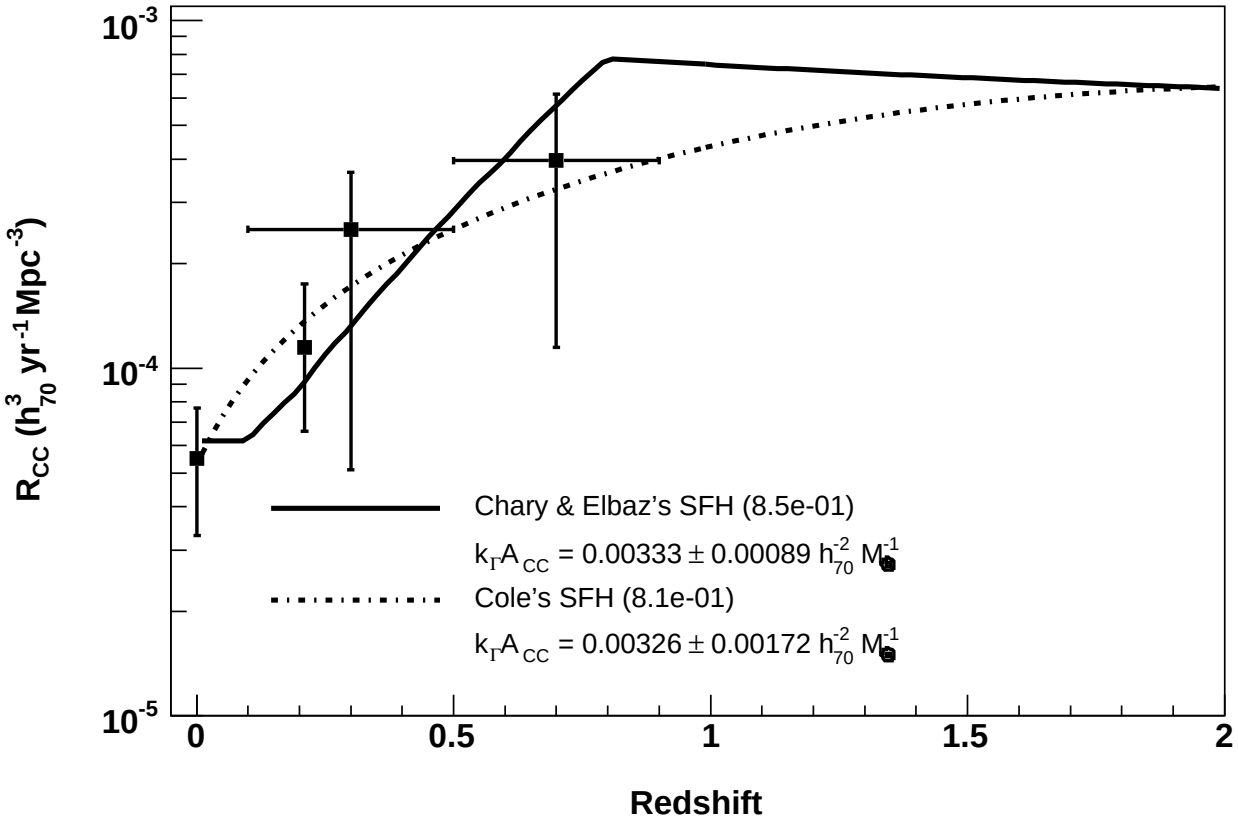

Fig. 7. Scaling of the SFH to the CCSN rate. Data are from Cappellaro et al. (1999) at $z \sim 0$, Botticella et al. (2008) at $z = 0.30$ and Dahlen et al. (2004) at $z = 0.3$ and $z = 0.7$ (see Tab. 2). The fitted value of $k_\Gamma A_{\rm CC}$ is shown; the χ^2 probability is in parenthesis.

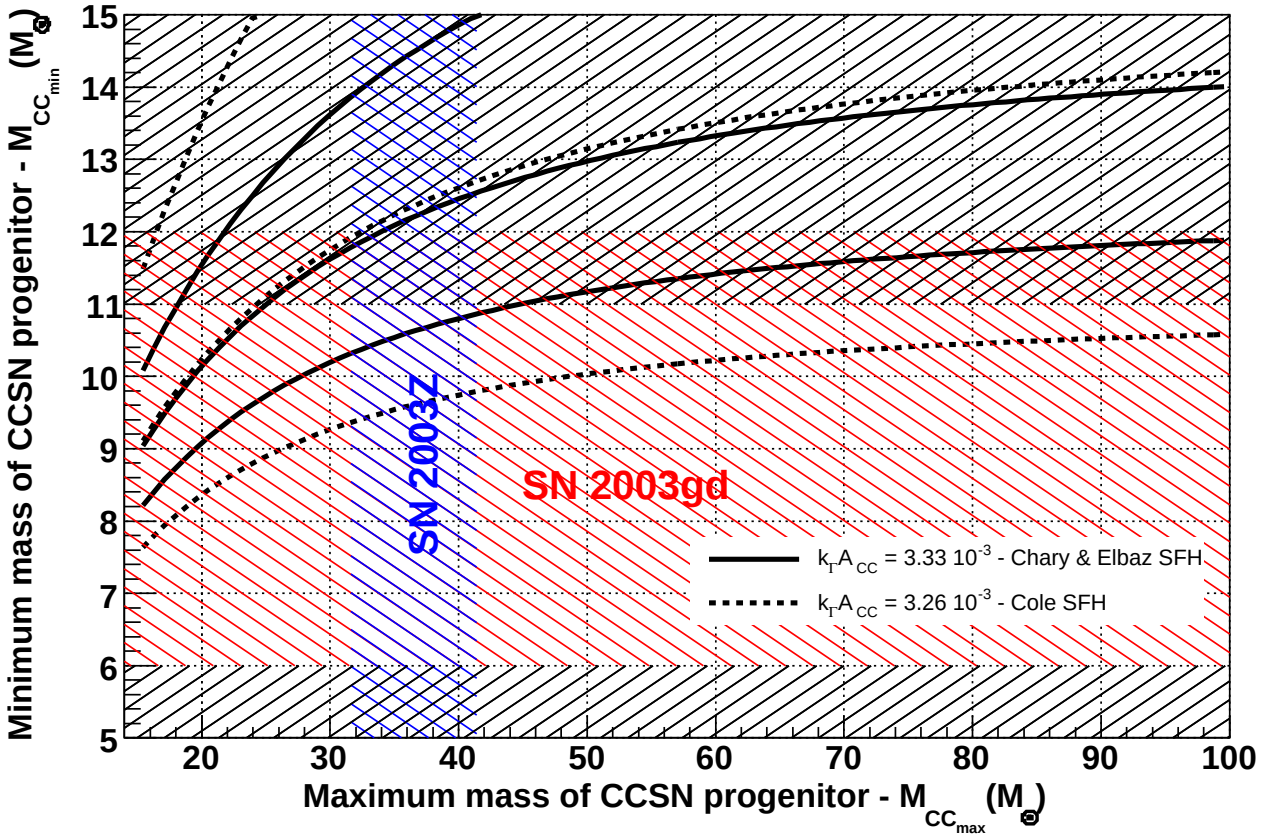

Fig. 8. Minimal CCSN progenitor mass as a function of the maximum mass, for two values of the scaling factor ($k_\Gamma A_{\rm CC}$) between CCSN rate and SFH, with their 1-σ error (the lines from top to bottom represent $k_\Gamma A_{\rm CC} - \sigma$, $k_\Gamma A_{\rm CC}$ and $k_\Gamma A_{\rm CC} + \sigma$ for both plotted values; $k_\Gamma A_{\rm CC}$ increases from top to bottom). Hatched zones (black parallel lines) reflect the theoretical "forbidden" area for the minimum CCSN progenitor mass, according to Heger et al. (2003); red and blue hatched areas stand respectively for SN 2003gd and SN 2003Z progenitor mass intervals.

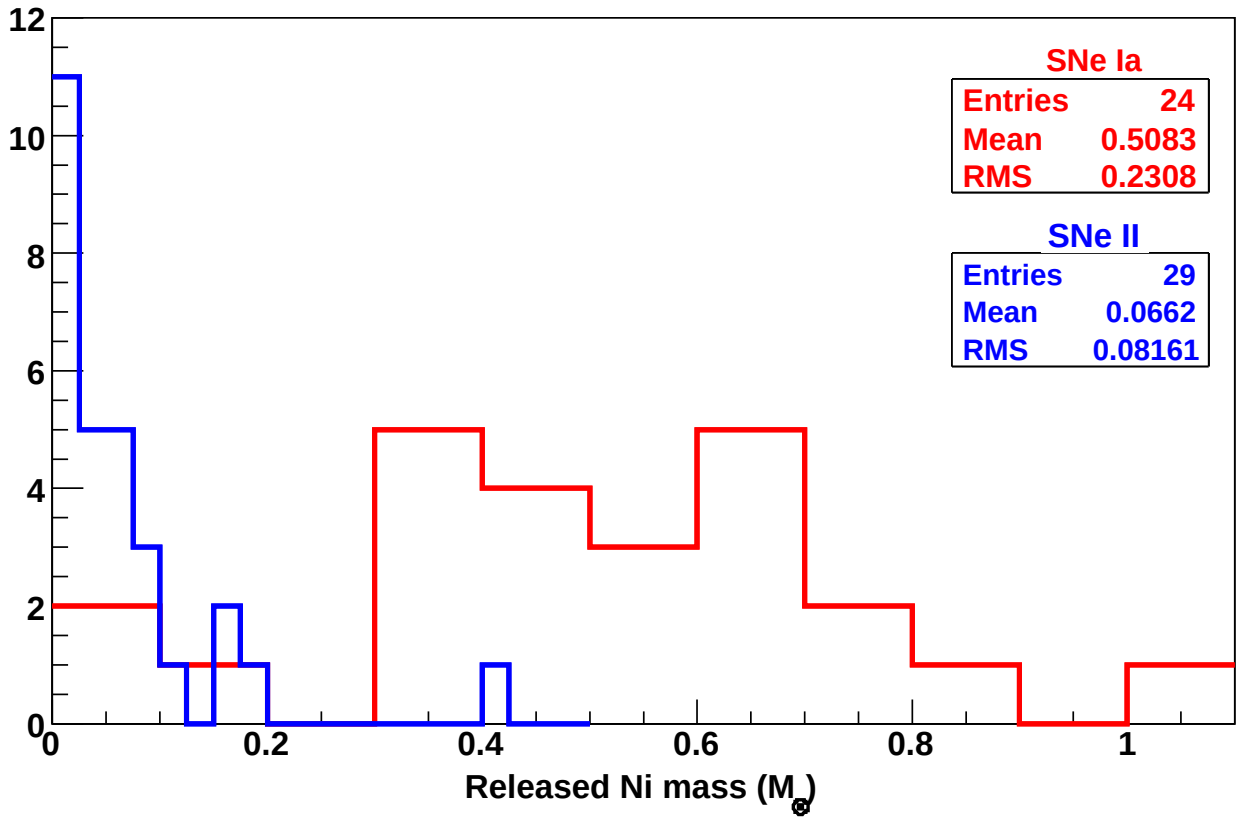

Fig. 9. Histogram of released ^{56}Ni mass, $\mathcal{M}_{^{56}\mathrm{Ni}}$, for type Ia SNe (Leibundgut 2000; Mazzali et al. 2000; Stritzinger et al. 2006); we took the mean value when necessary. And for type II SNe (Zampieri et al. (2003) and Hamuy (2003); we took the Zampieri et al. (2003) values for identical SNe in both sample).

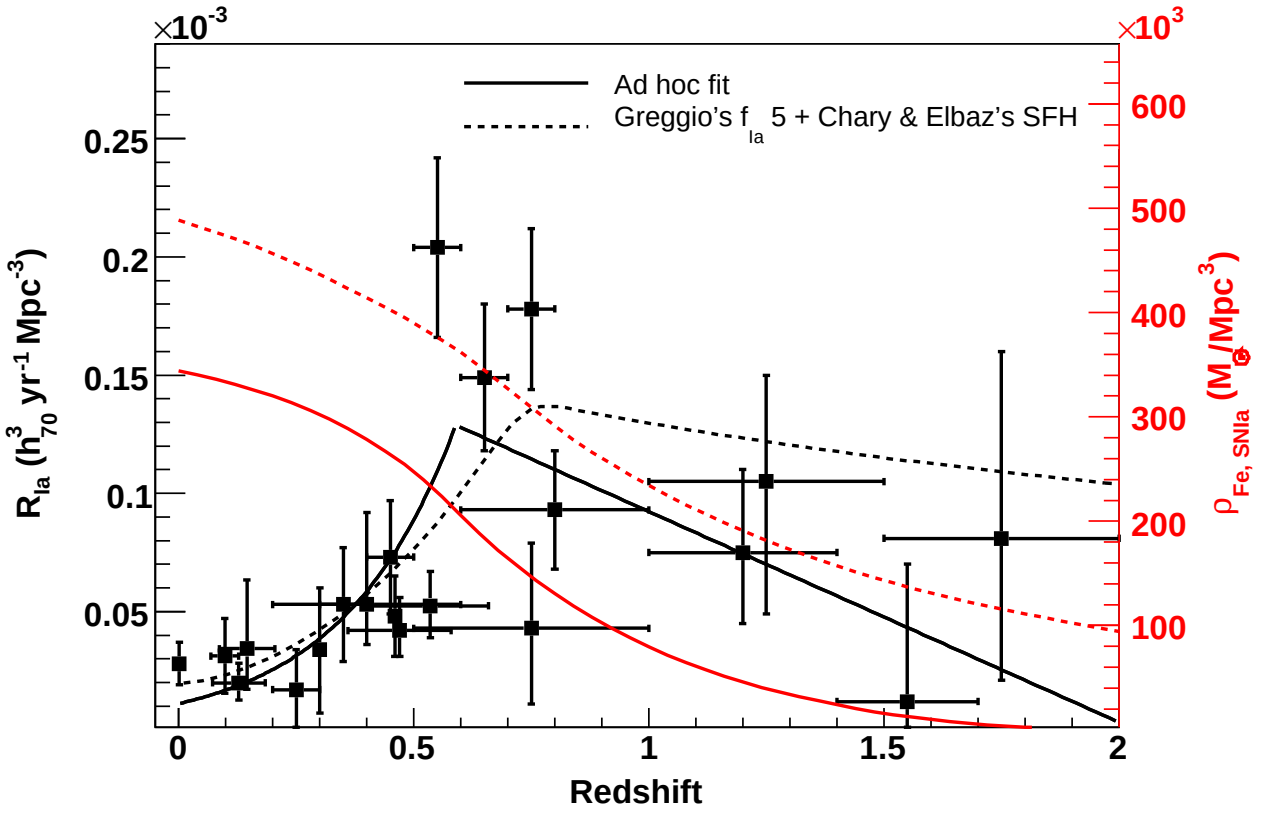

Fig. 10. Density of iron released by SNe Ia (in red, right scale) for two models of SN rate evolution. The SNIa rate measurements are superimposed (left scale) and fitted by an exponential between $z = 0$ and 0.59, and by a straight line for $z > 0.59$, or modeled by the Greggio SD_{subCh} delay time distribution convolved with the CE SFH (in black, left scale).

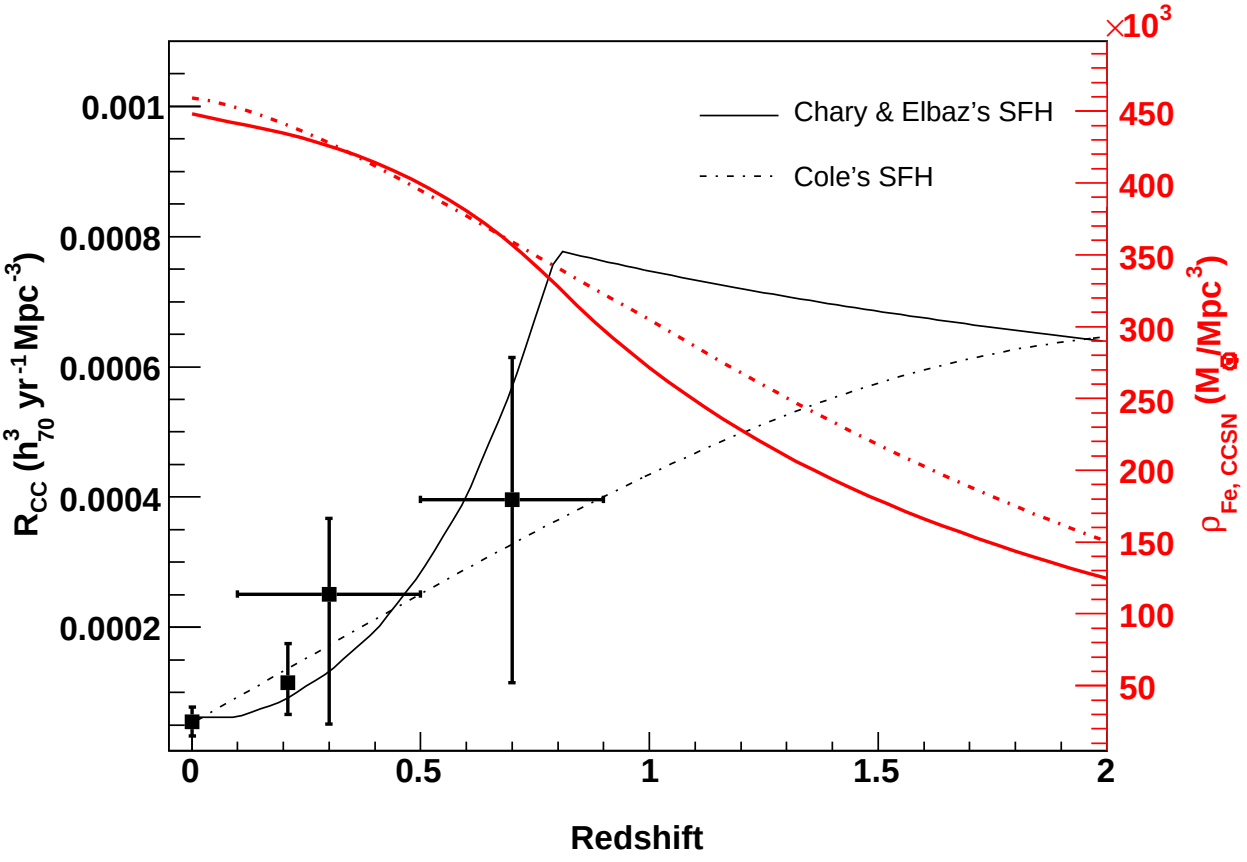

Fig. 11. Density of iron released by CCSNe (in red, right scale) as computed using different SFR models to fit the CCSN rate (in black, left scale). The first stars formation redshift is set to 20.

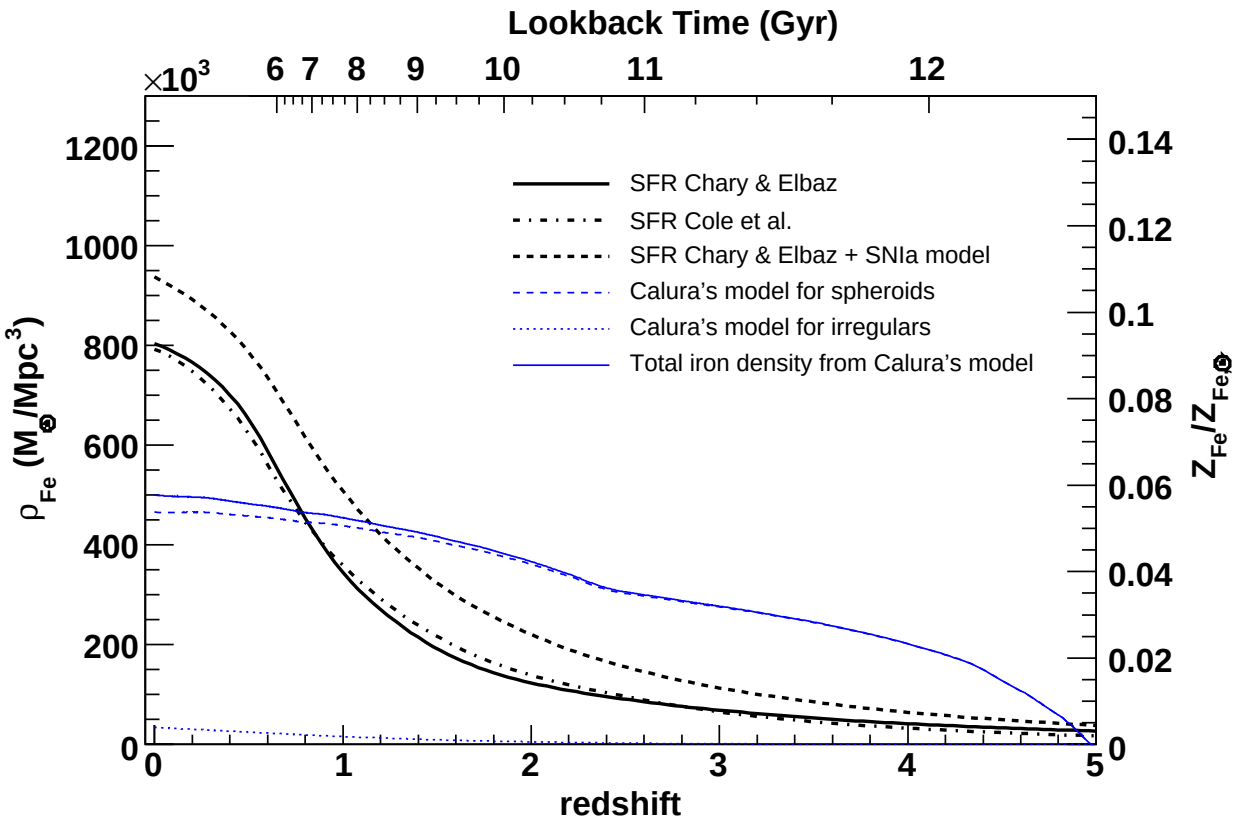

Fig. 12. Density of Fe released by both type Ia and CCSNe (for different SFH models) as a function of redshift (in black). The epoch of the first star explosions is set to $z = 20$. Right axis shows the corresponding iron mass abundance. Also shown (in blue) is the model by Calura & Matteucci (2006) of produced iron evolution, for dwarfs and irregular galaxies (dots), for spheroids (dashes) and in total (solid).

$\langle z \rangle$	SNIa rate [a]		$(\Omega_{M_\circ}, \Omega_{\Lambda_\circ})$	SNe	survey	limiting	spectro	author
	(h_{70}^2 SNu)	(10^{-5} h_{70}^3 Mpc^{-3} yr^{-1})		nb	surface	mag	confirmed	
0.38	$0.40^{+0.26+0.18}_{-0.18-0.12}$	-	(1.0, 0.0)	3	1.7 deg^2	$R \sim 23$	100 %	Pain et al. (1996)
0.01	0.18 ± 0.05	2.8±0.9		70	10^4 gal.	$B \sim 20$	100 %	Cappellaro et al. (1999)[b]
0.14	$0.22^{+0.17+0.06}_{-0.10-0.03}$	$3.43^{+2.7+1.1}_{-1.6-0.6}$	(0.3, 0.0)	4	80 deg^2	$V = 21.5$	100 %	Hardin et al. (2000)[b,c]
0.55	$0.28^{+0.05+0.05}_{-0.04-0.04}$	$5.25^{+0.96+1.10}_{-0.86-1.06}$	(0.3, 0.7)	38	12 deg^2	$R \sim 24.5$	100 %	Pain et al. (2002)
0.55	$0.46^{+0.08+0.07}_{-0.07-0.0.7}$	$11.1^{+2.0+1.1}_{-1.8-1.1}$	(1.0, 0.0)	38				Pain et al. (2002)
0.098	0.196 ± 0.098	3.12 ± 1.58		19	10^5 gal	$V > 20.4$	100 %	Madgwick et al. (2003)[b]
0.46	-	4.8 ± 1.7	(0.3, 0.7)	8	2.5 deg^2	$I \sim 24$	100 %	Tonry et al. (2003)
0.13	$0.125^{+0.044+0.028}_{-0.034-0.028}$	$1.99^{+0.70+0.47}_{-0.54-0.47}$	(0.3, 0.7)	14	598 deg^2	$V \sim 21$	100 %	Blanc et al. (2004)
[0.2, 0.6]	-	$6.9^{+3.4+15.4}_{-2.7-2.5}$	(0.3, 0.7)	3				Dahlen et al. (2004)
[0.6, 1.0]	-	$15.7^{+4.4+7.5}_{-2.5-5.3}$	(0.3, 0.7)	14	300 arcmin^2	$Z \sim 25.9$	76 %	Dahlen et al. (2004)
[1.0, 1.4]	-	$11.5^{+4.7+3.2}_{-2.6-4.4}$	(0.3, 0.7)	6				Dahlen et al. (2004)
[1.4, 1.8]	-	$4.4^{+3.2+1.4}_{-2.5-1.1}$	(0.3, 0.7)	2				Dahlen et al. (2004)
[0.2, 0.3]		1.7 ± 1.7	(0.3, 0.7)	1				Barris & Tonry (2006)[d]
[0.3, 0.4]	-	5.3 ± 2.4	(0.3, 0.7)	5				Barris & Tonry (2006)[d]
[0.4, 0.5]	-	7.3 ± 2.4	(0.3, 0.7)	9	2.3 deg^2	$m \sim 24.2$	24 %	Barris & Tonry (2006)[d]
[0.5, 0.6]	-	20.4 ± 3.8	(0.3, 0.7)	29				Barris & Tonry (2006)[d]
[0.6, 0.7]	-	14.9 ± 3.1	(0.3, 0.7)	23				Barris & Tonry (2006)[d]
[0.7, 0.8]	-	17.8 ± 3.4	(0.3, 0.7)	28				Barris & Tonry (2006)[d]
0.47	$0.154^{+0.039+0.048}_{-0.031-0.033}$	$4.2^{+0.6+1.3}_{-0.6-0.9}$	(0.3, 0.7)	73	4 deg^2	$i' \sim 23.3$	100 %	Neill et al. (2006)[f]
[0.0, 0.5]	-	$0.0^{+2.4}_{-0.0}$	(0.3, 0.7)	0.0				Poznanski et al. (2007)[g]
[0.5, 1.0]	-	$4.3^{+3.6}_{-3.2}$	(0.3, 0.7)	5.5	900 arcmin^2	$z' = 26.3$	0 %	Poznanski et al. (2007)[g]
[1.0, 1.5]	-	$10.5^{+4.5}_{-5.6}$	(0.3, 0.7)	10				Poznanski et al. (2007)[g]
[1.5, 2.0]	-	$8.1^{+7.9}_{-6.0}$	(0.3, 0.7)	3				Poznanski et al. (2007)[g]
[0.2, 0.6]	-	$5.3^{+3.9}_{-1.7}$	(0.3, 0.7)	5.44				Kuznetsova et al. (2008)[g,h]
[0.6, 1.0]	-	$9.3^{+2.5}_{-2.5}$	(0.3, 0.7)	18.33	300 arcmin^2	$Z \sim 25.9$	76 %	Kuznetsova et al. (2008)[g,h]
[1.0, 1.4]	-	$7.5^{+3.5}_{-3.0}$	(0.3, 0.7)	8.87				Kuznetsova et al. (2008)[g,h]
[1.4, 1.7]	-	$1.2^{+5.8}_{-1.2}$	(0.3, 0.7)	0.35				Kuznetsova et al. (2008)[g,h]
0.30	-	$3.4^{+1.6+2.1}_{-1.5-2.2}$	(0.3, 0.7)	86	43000 gal	$R \sim 23$	30 %	Botticella et al. (2008)

Table 1

Published restframe type Ia supernova explosion rate measurements. These rates are given together with the mean redshift of the observed SNe and the cosmological model assumed (especially for distant values). The fifth to eighth columns give respectively: the number of supernovae from which the rate is computed; the effective surface of the survey, or the number of galaxies surveyed; the limiting magnitude of the survey and the fraction of spectroscopically confirmed supernovae. NOTES: *a*) Quoted error bar are first statistics, and second systematics; where only one is present, the systematic is not available; *b*) the value per comoving volume is derived from the value in SNu times the 2dF luminosity density (the error on the luminosity density is added quadratically to the systematic uncertainty if distinct); *c*) For a (0.3, 0.7) cosmology the rate decreases by less than 5 % (Hardin et al. 2000); *d*) Barris & Tonry (2006) do not provide systematic errors on their measurements; *f*) Neill et al. (2006) used the Ilbert et al. (2005) luminosity function to translate their rate in SNu; *g*) statistical and systematic errors are added in quadrature; *h*) Kuznetsova et al. (2008) include the SN sample from Dahlen et al. (2004) to compute their rate.

$\langle z \rangle$	$R_{\rm SNII/Ibc}$		$(\Omega_{M_\circ}, \Omega_{\Lambda_\circ})$	SNe	survey	limiting	spectro	author
	(h_{70}^2 SNu)	(10^{-5} h_{70}^3 Mpc^{-3} yr^{-1})		nb	surface	mag	confirmed	
~ 0	0.41 ± 0.17	4.8 ± 1.9		67	10^4 gal	$R \sim 20$	100 %	Cappellaro et al. (1999)[a]
0.26	$1.26^{+0.48}_{-0.39}$	$19.2^{+7.0}_{-6.1}$	(0.3, 0.7)	28.2	11300 gal	$V \sim 24.5$	20 %	Cappellaro et al. (2005)
$[0.1, 0.5[$		$25.1^{+8.8+7.5}_{-7.5-18.6}$	(0.3, 0.7)	6	300 arcmin^2	$Z \sim 25.9$	63 %	Dahlen et al. (2004)[b]
$[0.5, 0.9[$		$39.6^{+10.3+19.2}_{-10.6-26.0}$	(0.3, 0.7)	10				Dahlen et al. (2004)[b]
0.21		$11.5^{+4.3+4.2}_{-3.3-3.6}$	(0.3, 0.7)	86	43000 gal	$R \sim 23$	30 %	Botticella et al. (2008)[b,c]

Table 2
Published restframe CCSN explosion rate measurements. These rates are given together with the mean redshift or redshift range of the observed SNe and the cosmological model assumed. The fifth to eighth columns give respectively: the number of supernovae from which the rate is computed; the effective surface of the survey, or the number of galaxies surveyed; the limiting magnitude of the survey and the fraction of spectroscopically confirmed supernovae. NOTES: *a*) The rate is translated into volumetric units by using a luminosity density of galaxies as in Cappellaro et al. (2005) *b*) We give here the value corrected for extinction by the authors *c*) Botticella et al. (2008) include the SN sample from Cappellaro et al. (2005) to compute their rate.